Ore Geology Reviews 90 (2017) 226–242

Contents lists available at ScienceDirect

Ore Geology Reviews

journal homepage: www.elsevier.com/locate/oregeo

Metallogeny of the Chrome Ores of the Xerolivado-Skoumtsa Mine, Vourinos Ophiolite, Greece: Implications on the genesis of IPGE-bearing high-Cr chromitites within a heterogeneously depleted mantle section

E. Tzamos [a], A. Kapsiotis [b,*], A. Filippidis [a], A. Koroneos [a], G. Grieco [c], A. Ewing Rassios [d], N. Kantiranis [a], A. Papadopoulos [a], P.N. Gamaletsos [e,f], A. Godelitsas [g]

[a] Department of Mineralogy-Petrology-Economic Geology, School of Geology, Faculty of Sciences, Aristotle University of Thessaloniki, 541 24 Thessaloniki, Greece
[b] School of Earth Science and Geological Engineering, Sun Yat-sen University, 510 275 Guangzhou, PR China
[c] Department of Earth Sciences, Università degli Studi di Milano, Via Botticelli 23, Milano, Italy
[d] Institute of Geology and Mineral Exploration, 501 00 Kozani, Greece
[e] Department of Metallurgy and Materials Technology, School of Mining and Metallurgical Engineering, National Technical University of Athens, 157 80 Athens, Greece
[f] Center for Electron Nanoscopy, Technical University of Denmark, Kongens Lyngby, Denmark
[g] Faculty of Geology and Geoenvironment, National and Kapodistrian University of Athens, 15784 Athens, Greece

ARTICLE INFO

Article history:
Received 15 July 2016
Received in revised form 4 March 2017
Accepted 10 March 2017
Available online 16 March 2017

Keywords:
Platinum-group elements (PGE)
Chromian spinel (Cr-spinel)
Chromitites
Ophiolites
Vourinos
Greece

ABSTRACT

Chrome ore deposits comprise less than 1% of the volume of a pervasively serpentinized dunite body (~3.5 km^3) that constitutes the Xerolivado-Skoumtsa Mine of the Vourinos Ophiolite in northwestern Greece. Ores have been examined to aid determination of their geological mode of occurrence, their mineralogy and mineral chemistry (Cr-spinel and olivine), and platinum-group element (PGE) geochemistry. The ore bodies are highly deformed and of the schlieren type, where Cr-spinel-rich and serpentine (after olivine)-rich layers (1–20 cm thick) alternate. The Cr-spinel displays a limited range in Cr# [100 × Cr/(Cr + Al)] atomic ratio (77–85) and TiO_2 content (0.05–0.22 wt%). The Mg# [100 × Mg/(Mg + Fe^{2+})] of Cr-spinel shows a wider variation (52–74) indicating that subsolidus (Mg_{Sp}-$Fe^{2+}{}_{Ol}$) re-equilibration occurred. Remnant fresh olivine in the serpentine-rich layers is typical forsterite [Fo#: 100 × Mg/(Mg + Fe^{2+}) = 93–95]. The Cr-rich chromitite ores have total PGE and Au abundances that range between 74.3 and 205 ppb: they show a general enrichment in Ir and Ru over PPGE (Rh, Pt and Pd) resulting mostly in a negatively-sloping C1 chondrite-normalized PGE profile with a quite strong Ru peak. Field observations indicate that the schlieren banding of the deformed ore bodies is a tectonometamorphic feature acquired within ductile deformation of the ophiolitic slab. Geochemical calculations demonstrate that the parental melts of the Xerolivado-Skoumtsa high-Cr chromitites were boninitic. Their high Ru content and variation in $Cr\#_{Sp}$ values indicate a polygenetic origin from geochemically similar, but spatially distinct melt inputs. These melts originated within a hydrated mantle wedge beneath a forearc basin within an evolving lithospheric slab. We emphasize that the PGE budget of the Xerolivado-Skoumtsa chromitites was not inherited from interactions of the migrating melts with their parental harzburgites, but it is an intrinsic feature of the deep-seated and heterogeneously depleted mantle source of these magmas.

1. Introduction

Ophiolites represent 'fossilized' fragments of old oceanic lithosphere tectonically emplaced onto continental margins during major orogenic events (e.g., Anonymous, 1972). The mantle section and/or the mantle-crust transition zone of ophiolite sequences contains chromian spinel (hereafter Cr-spinel) in restite harzburgite and dunite bodies (of residual to magmatic origin) as disseminated phases, and within dunite-hosted ore bodies as chromitites (e.g., Ahmed and Arai, 2002; Pagé and Barnes, 2009): economically viable ore bodies may contain anywhere from ~10% to 90% modal Cr-spinel. The morphology of the ore bodies is highly variable; from 'pod' shaped to strict tabular structures and diffuse disseminated deposits; despite the applicable structural terminology, they are commonly referred to as 'podiform' chrome deposits to distinguish them from the chrome ores of layered igneous intrusions

* Corresponding author.
E-mail addresses: kapsiotisa@yahoo.gr, kapsiotis@mail.sysu.edu.cn (A. Kapsiotis).

http://dx.doi.org/10.1016/j.oregeorev.2017.03.013
0169-1368/

(e.g., Arai, 1997a,b). The metallogenesis of oceanic lithospheric chrome deposits remains puzzling. A seemingly critical aspect within classic models for ophiolitic chromitites necessitates a 'blending' of hydrous melts of different SiO_2 concentrations (Arai and Yurimoto, 1994; Matveev and Ballhaus, 2002). Other theories favor chromitite formation caused by harzburgite-melt interaction followed by effective melt-melt mixing in permeable dunite channels (e.g., Arai, 1997a; Derbyshire et al., 2013; González-Jiménez et al., 2014a). Regardless of the potential mechanism of their formation, ophiolitic chromitites are still thought to be more characteristic of the lithospheric mantle in supra-subduction zones (SSZ; Arai and Yurimoto, 1995; Zhou et al., 1996) than within mid-ocean ridge- (MOR-) lithospheres (e.g., Arai and Miura, 2016).

Chromitites in ophiolites generally contain relatively high concentrations of platinum-group elements (PGE: Os, Ir, Ru, Rh, Pt and Pd) and Au, commonly in the order of 10–1000 ppb: such concentrations permit the study of the way in which partial melting has mobilized and concentrated these precious metals in the upper mantle (e.g., O'Driscoll and González-Jiménez, 2016 and references therein). Ophiolitic chromitites display a nearly ubiquitous enrichment in the refractory/compatible IPGE (Ir-group PGE: Os, Ir and Ru; melting points above 2300 °C) over the more fusible/incompatible PPGE (Pt-group PGE: Rh, Pt and Pd; melting points below 2000 °C; Barnes et al., 1985), regardless of the total PGE abundance (typically sub-chondritic to chondritic; e.g., Ahmed and Arai, 2002; González-Jiménez et al., 2014b). This compositional feature is attributed to the crystallization of chromitites from S-undersaturated melts derived from a mantle source that had its PPGE budget removed during an early episode of partial melting (e.g., Hamlyn and Keays, 1986; Keays, 1995; O'Hara et al., 2001). It has been proposed that the hydrated mantle wedge above a downgoing slab may be the ideal petrological environment for the production of S-undersaturated arc-type melts that tend to be variably rich in IPGE (e.g., Ahmed and Arai, 2002; Kapsiotis et al., 2009).

Herein, we re-examine six high-Cr chromitite bodies from the southern sector of the Xerolivado-Skoumtsa mine, Vourinos ophiolite complex (NW Greece). The principal goals of this renewed investigation are: i) to provide previously unpublished geological, mineral-chemical and geochemical data on these ore bodies; ii) to compare our results with those from older studies of ores from various localities within the mine in order to generate a more complete image of Cr mineralization within the Vourinos complex.

2. Geological background and field work

2.1. The Vourinos ophiolite complex

In Greece ophiolites occur as two NNW–SSE oriented nappes, namely the Jurassic 'Western Hellenic Ophiolites' (WHO) and the Jurassic-Early Cretaceous 'Eastern Hellenic Ophiolites' (EHO), placed to the west and east side of the Pelagonian platform, respectively (Fig. 1). Among the WHO, the Vourinos Ophiolite Complex in northwestern continental Greece (Fig. 1) represents a mid-Jurassic complete lithospheric slab of the Neo-Tethyan system emplaced (also in the mid-Jurassic) onto the passive margin of the Pelagonian continent (Moores, 1969; Smith and Rassios, 2003). This lithospheric section is about 12 km thick and outcrops over an area of 450 km^2. It is dominated by depleted harzburgite mantle tectonite (85% of the ophiolite exposures; Fig. 2) that hosts abundant, irregularly shaped and highly deformed bodies of dunite ranging in size from several m to km-scale lengths. Many of these dunite bodies contain small outcrops and ore-level concentrations of chromitites. Harzburgite and dunite are intruded by pyroxenite pegmatite dykes thought to represent the latest remnant of early magmatic

Fig. 1. The distribution of ophiolites in the southernmost part of the Balkan Peninsula (modified from Vergely, 1976). Note that Western Hellenic Ophiolites (WHO) and Eastern Hellenic Ophiolites (EHO) are shown with different colors. Key to lettering: V, Vourinos (marked by the blue square); P, Pindos; O, Othris. (For interpretation of the references to color in this figure legend, the reader is referred to the web version of this article.)

fluids (Rassios and Dilek, 2009). The boundary between mantle rocks and ultramafic cumulates (dunite, wehrlite and pyroxenite cumulates) is delineated by a well-exposed 'petrological Moho' (Tsouka district; Jackson et al., 1975). In the Krapa Hill, ultramafic cumulates progressively grade to mafic cumulate sequences composed of gabbronorite and rare troctolite (Fig. 2; Rassios, 1981). As a result of rotation of the ophiolitic section, magmatic layering in the cumulate sequence is essentially vertical, with an 'up-section' direction towards the west; the upper parts of the cumulate section are intruded by dykes, grading to a typical sheeted (diabasic) dyke complex with dyke orientations perpendicular to magmatic layering in the cumulate sequence (Rassios and Dilek, 2009). A poorly-represented extrusive sequence including basaltic to andesitic massive flows and pillow lavas occurs '*in situ*' over the sheeted dyke complex. Boninite dykes are pervasive within the dyke complex (making up about 10–15% of the dyke population).

A tectonic-sedimentary mélange (Agios Nikolaos or Zavordas mélange; Fig. 2; Ghikas et al., 2010) occurs between the basal mantle harzburgite rocks and the carbonate rocks of the Pelagonian platform. The precise contact of this mélange is delineated by a garnet-bearing amphibolite sole (Fig. 2; Rassios and Moores, 2006). Amphibole $^{40}Ar/^{39}Ar$ dating of the sole yielded emplacement ages at 171 ± 4 Ma (Spray and Roddick, 1980). Supplementary U-Pb ion microprobe dating of zircons from gabbros and plagiogranites yielded weighted mean $^{206}Pb/^{238}U$ ages at 168.5 ± 2.4 and 172.9 ± 3.1 Ma, respectively, which is taken as the time of igneous accretion of the Vourinos crust (Liati et al., 2004).

2.2. Field observations and sampling

The chrome ore bodies of Xerolivado-Skoumtsa are located within the 'metalliferous zone' of Vourinos (Grivas et al., 1993). This zone hosts all economic concentrations of chrome ore and appears to comprise an incipient ductile thrust within the upper mantle section. Xerolivado-Skoumtsa is one of the world's largest ophiolite-hosted chrome deposits. The mine is located within a

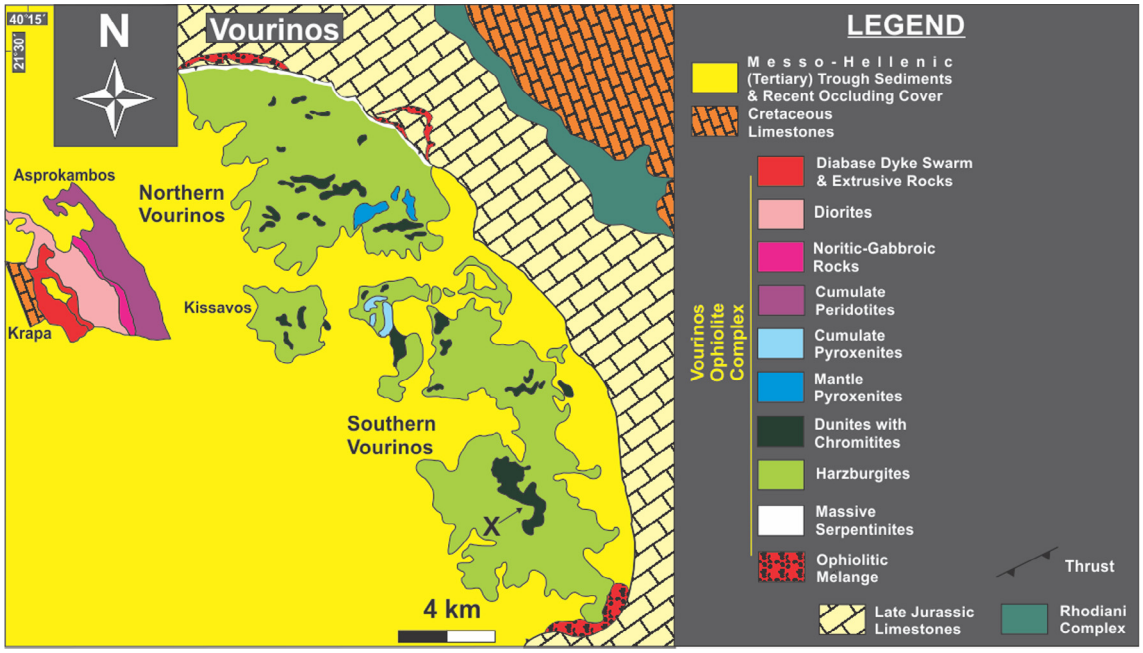

Fig. 2. Geological map of the Vourinos ophiolite complex showing the location of the study area (X: Xerolivado district; modified after Ghikas et al., 2010; Moores, 1969; Rassios, 1981).

dunite body (the largest known in Greece) with a surficial exposure of 3 × 1 km (Fig. 3). Chromitite occurs in seven distinct ore bodies.

Banded-type (schlieren) chrome ores form the bulk of the economic deposits of the Xerolivado-Skoumtsa Mine. These ore bodies

Fig. 3. Geological map of the Xerolivado-Skoumtsa dunite body showing surficial chromitite occurrences (modified after Grivas et al., 1986). The location of the investigated samples is also marked. The Xerolivado-Skoumtsa Mine is underground, between the Xerolivado and Skoumtsa localities.

are always enclosed by dunite envelopes, which are in turn surrounded by harzburgite-dunite folded intercalations. The ore bodies consist of deformed layers of chromitite (1–20 cm thick) and low modal Cr-spinel serpentinite (after dunite; Fig. 4a and b), giving rise to a typical 'schlieren texture' (Fig. 4a). The strike of the chromitite layers is approximately southwest-northeast and the dip is quite variable, but a stereogram of these indicates that the chromitite layers are generally folded (Fig. 4c) with an approximately southwest-dipping fold axis parallel to Cr-spinel lineation. Chrome ores tend to be associated with fold hinge-zones, and are thinned on the limbs. There seem to be no correlation between the thickness of chromitite bands with that of adjacent serpentinite bands (Fig. 4a). Chromitite layers commonly anastomose (Fig. 4b) and coalesce laterally but sometimes may be attenuated and discontinuous. These morphologies are more likely the result of complex ductile deformation rather than original magmatic features. Chromitite layers may be folded as a result of ductile deformation. Some isolated layers resemble Cr-spinel (and orthopyroxene) segregations due to mantle flow (Fig. 4d), and others show a strong metamorphic fabric (Fig. 4e) being foliated and lineated. When offset by small ductile faults, the thickness of chromitite bands appears to vary on each side of the fault-plane (Fig. 4f). Brittle fractures are imprinted on the deposits and host rocks. These fractures are generally vertical with respect to the orientation of chromitite layers. Most of them are filled by calcite (probably derived from penetration of ground waters originating in limestone).

Relatively small chromitite bodies (≤1 m across) occur on the periphery of the larger schlieren deposits as discontinuous deposits. These appear to form within the low-stress zones of macroscopic-scale structures in dunites, such as boudin-necks or the hinge-zones of folds.

Pyroxenite pegmatite dykes (≤20 cm) cross cut both chromitites and their host dunites, and are undeformed by ductile tectonics.

Serpentinization is extensive within the Xerolivado-Skoumtsa dunite body: dunite away from the ore bodies may contain ~15% 'fresh' remnant olivine; fresh olivine within the ore zones is rare.

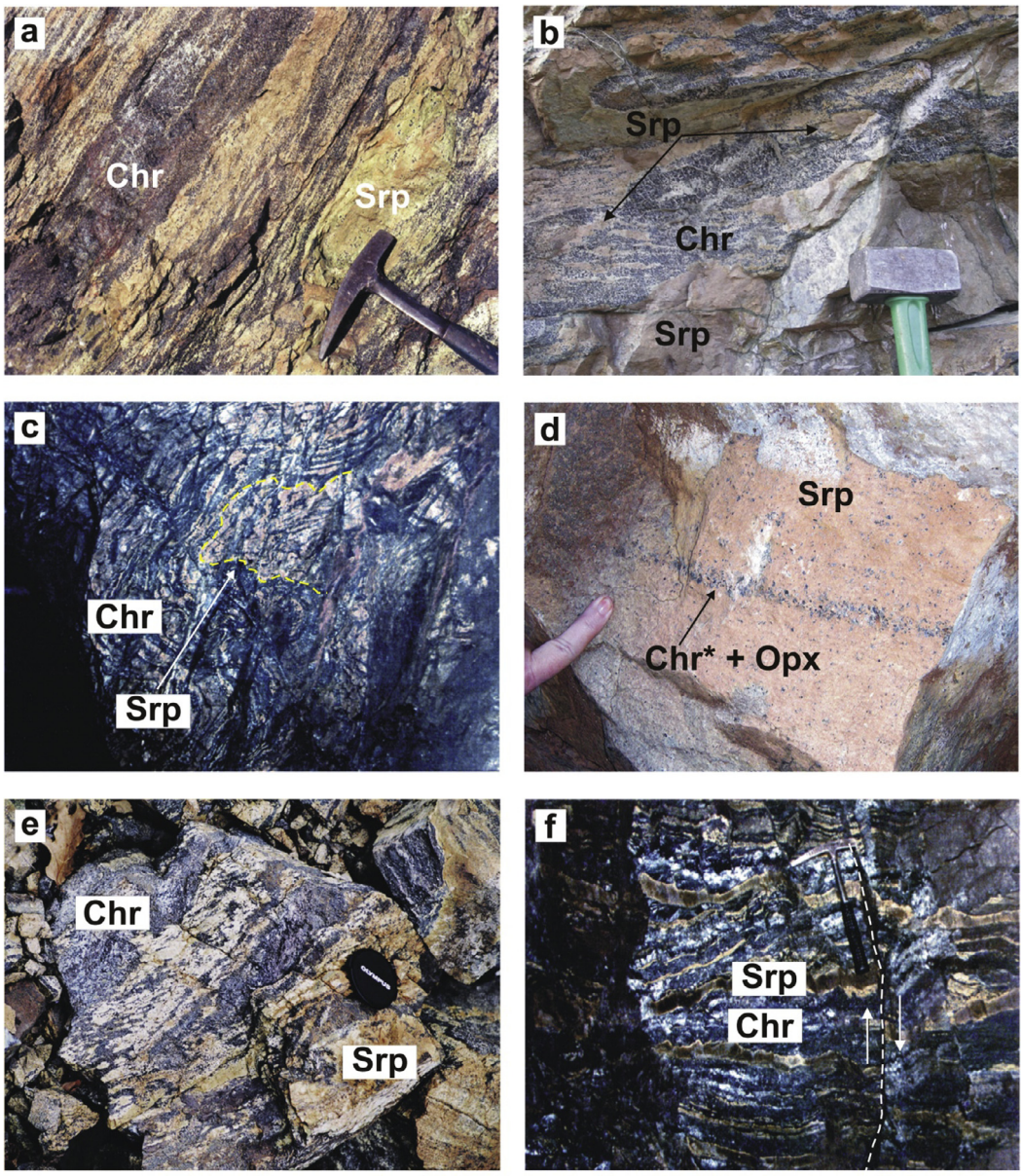

Fig. 4. Field photos showing the mode of occurrence of chromitites at the Xerolivado-Skoumtsa Mine. a) Typical 'schlieren' ore where chromitite bands alternate with serpentinite bands. b) Anastomosing chromitite layers. c) Multi-folded chromitite-serpentinite bands (the yellow dashed line marks the fold). d) Mantle flow in harzburgite resulting in concentration of orthopyroxene and chromian spinel (Cr-spinel) into a primary layer. e) Chromitite bands imprinted by ductile-phase strong crossing foliation and lineation. f) Offset of chromitite layers by a normal fault. Photos (c) and (f) were provided by K. Stamoulis and were taken from the mine galleries. Abbreviations: Chr – chromitite band; Chr* – Cr-spinel; Opx – orthopyroxene; Srp – serpentinite band. (For interpretation of the references to color in this figure legend, the reader is referred to the web version of this article.)

In this study, 40 samples of schlieren-type ores were examined from a well-documented suite collected within the southern sector of the Xerolivado-Skoumtsa mine. These samples include 20 specimens of chromitite bands and 20 samples of serpentinite (after dunite) bands. All samples were collected on (or near) the same vertical section (Fig. 3).

3. Previous studies on the composition of the Xerolivado-Skoumtsa chromitites

The composition of Cr-spinel and the geochemistry of precious metals in the Xerolivado-Skoumtsa chromitites have been the subject of a number of investigations in the last three decades. Konstantopoulou and Economou-Eliopoulos (1991) documented that the Xerolivado-Skoumtsa chromitites are remarkably homogeneous in terms of their major element composition and especially $Cr\#_{Sp}$ [$100 \times Cr/(Cr + Al) = 79–84$). These authors established PGE contents of 55.6–236.4 ppb (mg/kg) within these ores. The majority of chromitites analyzed by Konstantopoulou and Economou-Eliopoulos (1991) showed a greater abundance of the Os + Ir sum relative to that of Ru, low Pd/Ir ($\leq$0.12), and Pt + Pd/IPGE ($\leq$0.42) ratios. They interpreted these geochemical signatures to indicate that the Xerolivado-Skoumtsa chromitites precipitated from arc-type magmas derived from partial melting of an already depleted and hydrated mantle source. The analyses of schlieren ores from two underground sectors of Xerolivado-Skoumtsa by Grammatikopoulos et al. (2011) demonstrated that the ores had a low PGE content (103.5–114.1 ppb). These authors modeled chromitite precipitation from a differentiating hybridized boninite-type melt.

4. Laboratory methods

Polished thin-sections were studied under transmitted and reflected light to characterize chromitite petrography. Back-scattered electron (BSE) images, and microprobe analyses of chromite and olivine were conducted using the JEOL 8200 electron probe micro-analyzer (EPMA), which is equipped with a wavelength dispersive spectrometer (WDS) at the University of Milan, Italy. Analytical conditions were: 15 kV accelerating voltage, 15 nA beam current, 2 μm beam diameter with a counting time of 20 s on the peaks and 10 s on the background. Analyses of both Cr-spinel and olivine were done using the *Kα* lines for Mg, Si, Ca, Al, Ti, V, Cr, Mn, Fe, Ni and Zn. Standards used were a series of natural minerals (wollastonite for Si, forsterite for Mg, ilmenite for Ti, fayalite for Fe, anorthite for Al and Ca, chromite for Cr, niccolite for Ni, rhodonite for Mn and Zn, and metallic V for the homonymous element). The detection limit for all analyzed oxides was approximately 0.01 wt%. For each sample, 4–15 Cr-spinel cores and 1–6 olivine spots were analyzed and their compositions averaged to produce a statistical result. The FeO and Fe_2O_3 concentrations were calculated from FeO^t assuming ideal spinel stoichiometry ($RO:R_2O_3 = 1:1$). The majority of Cr-spinel analyses from both types of bands have been presented in a previous study dealing with the impact of re-equilibration phenomena on the composition of the Xerolivado-Skoumtsa chromitites (Tzamos et al., 2016). In the present study, we use electron microprobe data to constrain the origin of the chromitites. These mineral-chemical analyses of Cr-spinel from the ore bands are given in Tables 1 (chromitites) and 2 (serpentinized dunite), and the analyses of unaltered olivine from the serpentinite bands are given in Table 3.

Seven chromitite samples were analyzed for highly siderophile elements (HSE: PGE + Au) at the Activation Laboratories Ltd., Ontario, Canada by Instrumental Neutron-Activation Analysis (INAA) after a pre-concentration stage with nickel sulfide fire-assay collection. Detection limits were: 2 ppb for Os and Pd, 0.1 ppb for Ir, 5 ppb for Ru and Pt, 0.2 ppb for Rh and 0.5 ppb for Au. Three chromitite samples (C3/717B, C5/738 and C10/959) were analyzed for PGE and Au at the Acme Labs, Rustenburg, South Africa by nickel sulfide collection fire-assay with inductively coupled plasma-mass spectrometry (ICP-MS) finish; the detection limit was 1 ppb for all analyzed elements. Whole-rock PGE and Au contents of the chromitites are listed in Table 4.

5. Petrography

Chromitite ores of Xerolivado-Skoumtsa consist of more than 70% (modal) fine- to coarse-grained sintered cumulus Cr-spinel crystals. Chromian spinels are large (≤ 0.5 cm in diameter), subhedral to euhedral in morphology, and reddish to black (Fig. 5a). Any primary igneous features of the chromitites have been obliterated by high-*T* recrystallization, and an imprint of brittle pull-apart texture is observed implying deformation of the ores in a variety of *P-T* conditions. The Cr-spinel grains are generally extensively fractured (Fig. 5b), and some have undergone strong cataclasis; this cataclasis has altered the Cr-spinel to porous ferrian chromite, especially along cracks and grain boundaries (Fig. 5c). Such alteration has been documented by previous studies (Grieco and Merlini, 2012; Kapsiotis, 2015).

The intergranular silicate groundmass within the ores is almost entirely altered to serpentine (Fig. 5d) and minor chlorite. Some remnant grains of deformed and unaltered olivine have been located in clusters within serpentinized dunite bands (Fig. 5e). Occasionally these olivine clusters are surrounded by intergrowths of serpentine with brucite (Fig. 5f). Serpentine shows a typical mesh texture preserving the original 'mosaic' grain morphology of olivine (Fig. 5d) and, in very rare instances, minor bastite orthopyroxene is observed. The grain sizes of the original olivine preserved in this mosaic texture varies between 20 and 150 μm: this variation is especially well developed in the mesh-textured domains within the serpentinite bands. Chlorite forms brown blades intergrown with serpentine and ferrian chromite. The ores show limited evidence of subaerial weathering: when present, this takes the form of brown to reddish iddingsite aggregates (Fig. 5d and g).

Chromian spinel is also found disseminated (~3%–8% modal) in the serpentinite bands within the ores. Compared to the Cr-spinel from the chromitite bands, the disseminated Cr-spinels display a higher degree of alteration to ferrian chromite. Late calcite veins (≤200 μm thick, introduced by local groundwater) overprint all the aforesaid textural features.

Chromian spinel grains in chromitite bands contain small inclusions (ranging in size from 5 μm to 100 μm) of the following silicates: primary olivine, enstatite, diopside, and pargasite, and secondary alteration silicates of serpentine, chlorite, and hydrogrossular garnet. Some composite inclusions of orthopyroxene-amphibole intergrowths have been identified. The inclusions are subhedral to euhedral in shape, and seem randomly distributed among the Cr-spinel grains of the chromitite mass.

Grains of (secondary) accessory base metal minerals (BMM) were located dispersed within the serpentinite bands and, more rarely, scattered within the altered mesostasis of the chromitite bands (Fig. 5h). The most common BMM identified include: awaruite, heazlewoodite, magnetite and Co-bearing pentlandite.

6. Mineral chemistry

6.1. Chromian spinel (Cr-spinel or chromite) chemistry

The chemistry of Cr-spinels from both chromitite and serpentinite bands has been analyzed (Tables 1 and 2). The composition of Cr-spinel from the chromitite bands varies in Cr_2O_3 (58.58–63.87 wt%), Al_2O_3 (7.36–12.14 wt%), MgO (11.61–15.24 wt%) and FeO (9.66–16.05 wt%), being analogous to that observed in the chromitites from other ophiolites (Fig. 6a, Bonavia et al., 1993). Chromian spinel from the serpentinite bands shows a quite similar compositional variation (Cr_2O_3 = 58.67–61.61 wt%, Al_2O_3 = 7.37–11.89 wt%, MgO = 10.45–14.52 wt%, FeO = 11.67–17.06 wt%). Minor element oxide contents in Cr-spinel from the chromitite bands are generally low (TiO_2 = 0.05–0.20 wt%; V_2O_3 = 0.02–0.16 wt%; MnO ≤ 0.14 wt% and NiO ≤ 0.24 wt%), as is typical for mantle-hosted ophiolitic chromitites elsewhere. Minor element oxide contents in Cr-spinel from the serpentinite bands are similarly low (TiO_2 = 0.08–0.22 wt%; V_2O_3 = 0.04–0.17 wt%; MnO ≤ 0.21 wt% and NiO ≤ 0.17 wt%). Chromitite bands have Cr-spinel with high Cr# (77–85) and Mg# [100 × Mg/(Mg + Fe^{2+})= 57–74], similar to the more disseminated Cr-spinel from the serpentinite bands (Cr# = 77–85; Mg# = 52–69). Such compositions correspond to a classification of magnesiochromite for these Cr-spinels (Fig. 6b).

The Xerolivado-Skoumtsa chromitites are classified as high-Cr or metallurgical type chromitites ($Cr\#_{Sp} > 0.60$; Leblanc and Nicolas, 1992). The high Cr/Cr + Al and Mg/Mg + Fe^{2+} ratios of their Cr-spinel are comparable with those of accessory spinels within boninitic lavas (Dick and Bullen, 1984; Fig 6b). In the Cr/Cr + Al *vs.* Ti (Fig. 6c) and Al_2O_3 *vs.* TiO_2 (Fig. 6d) discrimination diagrams (Arai, 1997b; Kamenetsky et al., 2001), our analyses of Cr-spinel from the Xerolivado-Skoumtsa chromitites plot in the field of spinels in equilibrium with low-Ti arc-type (boninitic) melts.

Table 1
Average composition and structural formulae of Cr-spinel in the chromitite bands. Atomic ratios: Cr# [=100 × Cr/(Cr + Al)]; Mg# [=100 × Mg/(Mg + Fe^{2+}]; Fe^{3+}# [Fe^{3+}/(Fe^{3+} + Cr + Al)]; $Fe^{3+}/\Sigma Fe$ [Fe^{3+}/(Fe^{2+} + Fe^{3+})].

Composition of Cr-spinel from the chromitite bands										
Sample	C1/745	C3/692	C3/717A	C3/717B	C3/739	C3/750	C3/800	C4/692	C4/717A	C4/738
Number of analyses	(4)	(7)	(4)	(4)	(7)	(4)	(4)	(14)	(4)	(11)
SiO_2 (wt%)	0.05	0.03	0.04	0.03	0.01	0.02	0.03	0.02	0.02	0.01
TiO_2	0.13	0.12	0.15	0.15	0.15	0.17	0.16	0.15	0.13	0.16
Al_2O_3	10.21	8.67	9.05	10.94	8.85	11.98	11.57	8.17	8.59	9.47
Cr_2O_3	59.22	61.03	60.74	59.53	61.21	59.48	59.82	61.28	60.56	61.03
V_2O_3	0.10	0.09	0.12	0.09	0.10	0.08	0.08	0.09	0.07	0.11
$Fe_2O_3^*$	3.05	4.20	3.87	3.18	4.48	2.58	2.75	4.44	4.25	3.55
FeO	15.60	11.45	11.65	12.62	11.13	12.15	11.83	12.16	13.19	12.95
MnO	0.07	0.03	0.06	0.05	0.05	0.03	0.06	0.06	0.08	0.07
MgO	11.76	14.25	14.16	13.81	14.60	14.34	14.42	13.75	13.11	13.53
NiO	0.05	0.07	0.04	0.07	0.09	0.06	0.15	0.07	0.04	0.07
CaO	0.00	0.00	0.00	0.00	0.00	0.00	0.01	0.01	0.01	0.01
ZnO	0.03	0.01	0.00	0.05	0.01	0.05	0.04	0.03	0.00	0.05
Total	100.26	99.96	99.87	100.54	100.68	100.93	100.93	100.23	100.04	101.01
Structural formulae on the basis of 4 atoms of O										
Si	0.001	0.001	0.001	0.001	0.000	0.001	0.001	0.001	0.001	0.000
Ti	0.003	0.003	0.004	0.004	0.004	0.004	0.004	0.004	0.003	0.004
Al	0.392	0.331	0.345	0.412	0.334	0.446	0.431	0.312	0.330	0.358
Cr	1.526	1.561	1.553	1.504	1.551	1.486	1.496	1.573	1.560	1.549
V	0.003	0.002	0.003	0.002	0.002	0.002	0.002	0.002	0.002	0.003
Fe^{3+}	0.075	0.102	0.094	0.076	0.108	0.061	0.066	0.109	0.104	0.086
Fe^{2+}	0.425	0.310	0.315	0.337	0.298	0.321	0.313	0.330	0.360	0.348
Mn	0.002	0.001	0.002	0.001	0.001	0.001	0.002	0.002	0.002	0.002
Mg	0.571	0.687	0.682	0.658	0.698	0.675	0.680	0.665	0.637	0.647
Ni	0.001	0.002	0.001	0.002	0.002	0.001	0.004	0.002	0.001	0.002
Ca	0.000	0.000	0.000	0.000	0.000	0.000	0.000	0.000	0.000	0.000
Zn	0.001	0.000	0.000	0.001	0.000	0.001	0.001	0.001	0.000	0.001
Total	3.000	3.000	3.000	3.000	3.000	3.000	3.000	3.000	3.000	3.000
Cr#	79.55	82.52	81.82	78.49	82.28	76.91	77.62	83.43	82.55	81.21
Mg#	57.35	68.93	68.16	66.10	70.04	67.77	68.49	66.84	63.91	65.06
Fe^{3+}/(Fe^{3+} + Cr + Al)	0.04	0.05	0.05	0.04	0.05	0.03	0.03	0.05	0.05	0.04
$Fe^{3+}/\Sigma Fe$	0.15	0.25	0.23	0.19	0.27	0.16	0.17	0.25	0.23	0.20
Fe^{3+}/Fe^{2+}	0.18	0.33	0.30	0.23	0.36	0.19	0.21	0.33	0.29	0.25

Composition of Cr-spinel from the chromitite bands										
Sample	C4/765	C4/800	C5/717	C5/738	C5/692	C5/766	C6/692	C6/717	C6/741	C10/939
Number of analyses	(4)	(6)	(3)	(10)	(7)	(6)	(5)	(6)	(9)	(4)
SiO_2 (wt%)	0.01	0.02	0.02	0.25	0.01	0.02	0.28	0.01	0.02	0.01
TiO_2	0.13	0.15	0.16	0.14	0.14	0.15	0.14	0.12	0.14	0.14
Al_2O_3	9.29	9.69	8.87	9.62	8.86	10.27	8.62	8.35	9.85	11.06
Cr_2O_3	61.13	60.88	61.13	60.81	61.19	60.23	60.79	61.57	61.64	60.01
V_2O_3	0.09	0.10	0.12	0.10	0.07	0.08	0.10	0.10	0.09	0.10
$Fe_2O_3^*$	3.61	3.09	3.83	4.04	4.19	3.72	4.10	4.34	2.90	2.00
FeO	12.49	13.57	12.32	11.23	11.62	12.32	14.27	12.31	12.20	13.33
MnO	0.09	0.03	0.11	0.04	0.04	0.05	0.10	0.05	0.04	0.06
MgO	13.75	13.15	13.76	14.64	14.26	14.04	12.53	13.79	14.11	13.23
NiO	0.05	0.05	0.05	0.08	0.04	0.08	0.05	0.07	0.06	0.10
CaO	0.00	0.01	0.00	0.11	0.01	0.01	0.14	0.01	0.00	0.00
ZnO	0.03	0.02	0.01	0.01	0.03	0.01	0.01	0.03	0.03	0.12
Total	100.68	100.75	100.39	101.09	100.45	100.99	101.12	100.74	101.09	100.16
Structural formulae on the basis of 4 atoms of O										
Si	0.000	0.001	0.001	0.008	0.000	0.001	0.009	0.000	0.001	0.000
Ti	0.003	0.004	0.004	0.003	0.003	0.004	0.003	0.003	0.003	0.003
Al	0.352	0.368	0.338	0.360	0.336	0.386	0.329	0.318	0.370	0.419
Cr	1.555	1.551	1.561	1.529	1.557	1.518	1.556	1.571	1.554	1.526
V	0.002	0.003	0.003	0.003	0.002	0.002	0.003	0.002	0.002	0.003
Fe^{3+}	0.087	0.075	0.093	0.097	0.102	0.089	0.100	0.105	0.069	0.048
Fe^{2+}	0.336	0.366	0.333	0.299	0.313	0.328	0.386	0.332	0.325	0.359
Mn	0.003	0.001	0.003	0.001	0.001	0.001	0.003	0.001	0.001	0.002
Mg	0.659	0.632	0.663	0.694	0.684	0.667	0.605	0.664	0.671	0.634
Ni	0.001	0.001	0.001	0.002	0.001	0.002	0.001	0.002	0.002	0.003
Ca	0.000	0.000	0.000	0.004	0.000	0.000	0.005	0.000	0.000	0.000
Zn	0.001	0.001	0.000	0.000	0.001	0.000	0.000	0.001	0.001	0.003
Total	3.000	3.000	3.000	3.000	3.000	3.000	3.000	3.000	3.000	3.000
Cr#	81.53	80.83	82.22	80.93	82.25	79.74	82.56	83.18	80.77	78.45
Mg#	66.24	63.34	66.57	69.91	68.63	67.02	61.01	66.64	67.33	63.88
Fe^{3+}/(Fe^{3+} + Cr + Al)	0.04	0.04	0.05	0.05	0.05	0.05	0.05	0.05	0.04	0.02
$Fe^{3+}/\Sigma Fe$	0.21	0.17	0.22	0.25	0.25	0.21	0.21	0.24	0.18	0.12
Fe^{3+}/Fe^{2+}	0.26	0.21	0.28	0.32	0.33	0.27	0.26	0.32	0.21	0.14

Table 2
Average composition and structural formulae of Cr-spinel in the serpentinite bands. Atomic ratios: Cr# [=100 × Cr/(Cr + Al)]; Mg# [=100 × Mg/(Mg + Fe^{2+}]; Fe^{3+}# [=Fe^{3+}/(Fe^{3+} + Cr + Al)]; $Fe^{3+}/\Sigma Fe$ [=Fe^{3+}/(Fe^{2+} + Fe^{3+})].

Composition of Cr-spinel from the serpentinite bands										
Sample	C1/745	C3/692	C3/717A	C3/717B	C3/739	C3/750	C3/800	C4/692	C4/717A	C4/738
Number of analyses	(4)	(4)	(3)	(4)	(4)	(2)	(4)	(2)	(5)	(5)
SiO_2 (wt%)	0.02	0.03	0.04	0.06	0.01	0.08	0.02	0.00	0.03	0.01
TiO_2	0.12	0.15	0.16	0.16	0.15	0.16	0.17	0.14	0.14	0.14
Al_2O_3	10.06	8.48	8.38	10.74	8.61	11.83	11.39	8.61	8.14	9.47
Cr_2O_3	59.13	60.21	60.43	59.46	60.60	59.19	59.70	60.78	59.62	60.54
V_2O_3	0.11	0.08	0.10	0.12	0.10	0.11	0.09	0.11	0.09	0.11
$Fe_2O_3^*$	3.24	4.33	3.95	3.02	4.32	2.77	2.92	4.42	4.63	3.61
FeO	16.10	13.69	14.71	13.35	13.72	13.27	13.57	14.09	16.04	14.47
MnO	0.08	0.10	0.09	0.03	0.13	0.06	0.07	0.09	0.12	0.10
MgO	11.38	12.71	12.04	13.31	12.80	13.60	13.41	12.74	11.14	12.55
NiO	0.05	0.04	0.06	0.08	0.09	0.11	0.08	0.01	0.05	0.05
CaO	0.01	0.00	0.01	0.01	0.00	0.00	0.01	0.00	0.00	0.00
ZnO	0.11	0.02	0.05	0.01	0.02	0.07	0.06	0.00	0.06	0.05
Total	100.40	99.84	100.03	100.35	100.55	101.23	101.47	100.98	100.06	101.10
Structural formulae on the basis of 4 atoms of O										
Si	0.001	0.001	0.001	0.002	0.000	0.002	0.001	0.000	0.001	0.000
Ti	0.003	0.004	0.004	0.004	0.004	0.004	0.004	0.003	0.003	0.003
Al	0.387	0.327	0.324	0.407	0.330	0.442	0.426	0.329	0.318	0.360
Cr	1.527	1.559	1.570	1.511	1.558	1.483	1.498	1.557	1.560	1.545
V	0.003	0.002	0.003	0.003	0.003	0.003	0.002	0.003	0.002	0.003
Fe^{3+}	0.080	0.107	0.098	0.073	0.106	0.066	0.070	0.108	0.115	0.088
Fe^{2+}	0.440	0.375	0.404	0.359	0.373	0.352	0.360	0.382	0.444	0.391
Mn	0.002	0.003	0.003	0.001	0.004	0.002	0.002	0.002	0.003	0.003
Mg	0.554	0.621	0.590	0.638	0.621	0.642	0.634	0.615	0.550	0.604
Ni	0.001	0.001	0.002	0.002	0.002	0.003	0.002	0.000	0.001	0.001
Ca	0.000	0.000	0.000	0.000	0.000	0.000	0.000	0.000	0.000	0.000
Zn	0.003	0.000	0.001	0.000	0.000	0.002	0.001	0.000	0.002	0.001
Total	3.000	3.000	3.000	3.000	3.000	3.000	3.000	3.000	3.000	3.000
Cr#	79.77	82.65	82.88	78.79	82.52	77.04	77.87	82.56	83.09	81.09
Mg#	55.75	62.33	59.34	63.98	62.45	64.62	63.78	61.70	55.30	60.70
Fe^{3+}/(Fe^{3+} + Cr + Al)	0.04	0.05	0.05	0.04	0.05	0.03	0.04	0.05	0.06	0.04
$Fe^{3+}/\Sigma Fe$	0.15	0.22	0.20	0.17	0.22	0.16	0.16	0.22	0.21	0.18
Fe^{3+}/Fe^{2+}	0.18	0.29	0.24	0.20	0.28	0.19	0.19	0.28	0.26	0.22

Composition of Cr-spinel from the serpentinite bands										
Sample	C4/765	C4/800	C5/717	C5/738	C5/692	C5/766	C6/692	C6/717	C6/741	C10/939
Number of analyses	6	4	3	6	2	3	3	3	2	4
SiO_2 (wt%)	0.03	0.02	0.04	0.02	0.02	0.04	0.01	0.03	0.01	0.02
TiO_2	0.16	0.14	0.18	0.16	0.14	0.11	0.14	0.14	0.12	0.14
Al_2O_3	8.91	9.20	8.88	9.94	8.88	10.10	8.24	8.08	9.84	10.72
Cr_2O_3	60.49	60.93	60.95	60.57	61.51	59.65	60.70	60.51	61.03	60.10
V_2O_3	0.08	0.07	0.12	0.10	0.12	0.10	0.11	0.08	0.17	0.12
$Fe_2O_3^*$	3.85	2.98	4.33	3.55	3.82	3.85	4.09	4.55	3.10	2.04
FeO	14.48	15.81	12.68	12.99	12.03	14.53	15.39	13.56	13.86	13.74
MnO	0.13	0.12	0.09	0.08	0.07	0.06	0.14	0.11	0.05	0.08
MgO	12.36	11.58	13.62	13.58	13.99	12.60	11.70	12.74	13.06	12.93
NiO	0.05	0.10	0.08	0.06	0.10	0.07	0.05	0.09	0.05	0.09
CaO	0.01	0.01	0.01	0.01	0.02	0.00	0.00	0.00	0.02	0.01
ZnO	0.05	0.06	0.06	0.02	0.02	0.06	0.02	0.00	0.07	0.05
Total	100.59	101.02	101.04	101.08	100.71	101.17	100.60	99.89	101.37	100.03
Structural formulae on the basis of 4 atoms of O										
Si	0.001	0.001	0.001	0.001	0.001	0.001	0.000	0.001	0.000	0.001
Ti	0.004	0.003	0.004	0.004	0.003	0.003	0.003	0.003	0.003	0.003
Al	0.342	0.353	0.337	0.375	0.337	0.383	0.318	0.312	0.372	0.408
Cr	1.557	1.568	1.550	1.532	1.564	1.517	1.574	1.569	1.546	1.535
V	0.002	0.002	0.003	0.003	0.003	0.003	0.003	0.002	0.004	0.003
Fe^{3+}	0.094	0.073	0.105	0.085	0.092	0.093	0.101	0.112	0.075	0.050
Fe^{2+}	0.394	0.430	0.341	0.348	0.323	0.391	0.422	0.372	0.371	0.371
Mn	0.004	0.003	0.003	0.002	0.002	0.002	0.004	0.003	0.001	0.002
Mg	0.600	0.562	0.653	0.648	0.671	0.604	0.572	0.623	0.624	0.623
Ni	0.001	0.003	0.002	0.002	0.003	0.002	0.001	0.002	0.001	0.002
Ca	0.000	0.000	0.000	0.000	0.001	0.000	0.000	0.000	0.001	0.000
Zn	0.001	0.001	0.001	0.001	0.001	0.001	0.000	0.000	0.002	0.001
Total	3.000	3.000	3.000	3.000	3.000	3.000	3.000	3.000	3.000	3.000
Cr#	82.00	81.63	82.16	80.35	82.29	79.85	83.18	83.41	80.62	79.01
Mg#	60.33	56.62	65.70	65.07	67.46	60.71	57.54	62.62	62.67	62.66
Fe^{3+}/(Fe^{3+} + Cr + Al)	0.05	0.04	0.05	0.04	0.05	0.05	0.05	0.06	0.04	0.03
$Fe^{3+}/\Sigma Fe$	0.19	0.15	0.24	0.20	0.22	0.19	0.19	0.23	0.17	0.12
Fe^{3+}/Fe^{2+}	0.24	0.17	0.31	0.25	0.29	0.24	0.24	0.30	0.20	0.13

Table 3
Average composition and structural formulae of olivine in the serpentinite bands. Atomic ratio: Fo# [=100 × Mg/(Mg + Fe^{2+}].

Composition of olivine from the serpentinite bands													
Sample	C1/745	C3/692	C3/717A	C3/739	C4/692	C4/717A	C4/738	C4/800	C5/717	C5/738	C6/692	C6/717	C6/741
Number of analyses	(3)	(1)	(4)	(5)	(1)	(2)	(1)	(2)	(2)	(3)	(4)	(1)	(6)
SiO_2	41.05	42.34	42.07	41.42	41.85	41.89	41.47	41.74	41.78	42.13	42.01	41.87	41.82
TiO_2	0.02	0.00	0.01	0.01	0.09	0.04	0.09	0.00	0.05	0.01	0.01	0.00	0.01
Al_2O_3	0.00	0.04	0.00	0.01	0.00	0.01	0.00	0.00	0.01	0.00	0.01	0.01	0.00
Cr_2O_3	0.02	0.02	0.02	0.01	0.00	0.01	0.04	0.02	0.02	0.01	0.01	0.03	0.02
V_2O_3	0.01	0.00	0.01	0.00	0.00	0.03	0.01	0.03	0.02	0.00	0.00	0.00	0.01
FeO	6.19	4.94	5.51	5.15	5.26	6.07	5.59	5.66	4.87	4.09	6.08	4.95	4.96
MnO	0.06	0.07	0.07	0.08	0.07	0.10	0.10	0.07	0.08	0.07	0.08	0.10	0.08
MgO	51.91	53.91	53.00	52.68	53.02	52.92	52.43	52.65	53.40	54.23	52.55	52.66	53.39
NiO	0.48	0.40	0.44	0.57	0.44	0.38	0.39	0.50	0.44	0.55	0.36	0.41	0.57
CaO	0.02	0.01	0.03	0.04	0.02	0.04	0.03	0.01	0.00	0.02	0.03	0.04	0.02
ZnO	0.04	0.00	0.00	0.02	0.00	0.03	0.00	0.00	0.02	0.05	0.05	0.00	0.01
Total	99.81	101.73	101.17	99.98	100.74	101.52	100.15	100.66	100.67	101.16	101.19	100.07	100.90
Structural formulae on the basis of 4 atoms of O													
Si	0.994	0.998	1.000	0.996	0.998	1.000	0.995	0.998	0.996	0.997	1.001	1.004	0.996
Ti	0.000	0.000	0.000	0.000	0.002	0.001	0.001	0.000	0.001	0.000	0.000	0.000	0.000
Al	0.000	0.001	0.000	0.000	0.000	0.000	0.000	0.000	0.000	0.000	0.000	0.000	0.000
Cr	0.000	0.000	0.000	0.000	0.000	0.000	0.000	0.000	0.000	0.000	0.000	0.001	0.000
V	0.000	0.000	0.000	0.000	0.000	0.001	0.001	0.001	0.000	0.000	0.000	0.000	0.000
Fe	0.125	0.097	0.110	0.104	0.105	0.141	0.121	0.113	0.097	0.081	0.121	0.099	0.099
Mn	0.001	0.001	0.001	0.002	0.001	0.002	0.002	0.001	0.002	0.001	0.002	0.002	0.002
Mg	1.873	1.895	1.878	1.889	1.885	1.847	1.875	1.877	1.898	1.912	1.866	1.881	1.895
Ni	0.009	0.008	0.008	0.011	0.008	0.006	0.007	0.010	0.008	0.010	0.007	0.008	0.011
Ca	0.001	0.000	0.001	0.001	0.001	0.001	0.001	0.000	0.000	0.000	0.001	0.001	0.001
Zn	0.001	0.000	0.000	0.000	0.000	0.001	0.001	0.000	0.000	0.001	0.001	0.000	0.000
Total	3.006	3.001	2.999	3.003	3.000	2.999	3.003	3.001	3.003	3.003	2.999	2.996	3.004
Fo#	93.1	94.6	94.0	94.1	94.2	93.4	93.8	93.8	94.6	95.3	93.4	94.4	94.4

Table 4
Whole-rock PGE and Au concentrations (ppb) in the Xerolivado-Skoumtsa chromitites.

Whole-rock PGE and Au concentrations											
Number of sample	Os (ppb)	Ir (ppb)	Ru (ppb)	Rh (ppb)	Pt (ppb)	Pd (ppb)	Au (ppb)	Pd/Ir	(Pt + Pd)/(Ir + Ru)	ΣPGE (ppb)	ΣPGE+Au (ppb)
Detection limits	**1**	**1**	**1**	**1**	**1**	**1**	**1**				
C3/717B	<1	23	36	<1	16	<1	58	–	0.27	75	133
C5/738	<1	18	37	<1	16	<1	35	–	0.29	71	106
C10/959	<1	18	36	<1	16	82	53	4.56	1.81	152	205
Detection limits	**2**	**0.1**	**5**	**0.2**	**5**	**2**	**0.5**				
C4/738	<2	24.2	66	7.4	<5	2	<0.5	0.08	0.02	99.6	99.6
C6/741	<2	26.9	92	7.8	<5	2	<0.5	0.07	0.02	128.7	128.7
C4/800	<2	19.2	52	5.6	<5	2	<0.5	0.10	0.03	78.8	78.8
C4/717	<2	21.5	48	6.1	<5	2	<0.5	0.09	0.03	77.6	77.6
C3/739	<2	27.7	105	9.1	<5	2	<0.5	0.07	0.02	143.8	143.8
C4/765	<2	21.2	46	5.1	<5	2	<0.5	0.09	0.03	74.3	74.3
C4/692	<2	30.1	72	8	<5	2	<0.5	0.07	0.02	112.1	112.1

6.2. Olivine chemistry

Remnant grains of olivine within serpentinite bands of the ore bodies have high forsterite (Fo) content (Fo# = 93–95; Table 3). The NiO content of these olivine grains varies from 0.29 to 0.61 wt%, showing an increase in NiO with increasing Fo# values (Fig. 7a). The MnO content ranges between 0.04 and 0.13 wt%, having no correlation with Fo# values (Fig. 7b). These olivine compositions deviate (Fig. 7a and b) noticeably from the known mantle olivine array (MOA; Ozawa, 1994).

7. PGE and Au geochemistry

The overall abundance of precious metals (ΣPGE + Au) in the Xerolivado-Skoumtsa chromitites ranges from 74.3 to 205 ppb: total PGE contents vary between 71 and 152 ppb and the maximum Au abundance is 58 ppb. These ores show enrichment in the IPGE (54–132.7 ppb) relative to the PPGE (7.1–98 ppb), categorizing them as type *I* chromitites (González-Jiménez et al., 2014a). Osmium is below the detection limits in all samples. With one exception, all chromitites are enriched in Ru (36–105 ppb); the exception, sample C10/959, is characterized by a high content of Pd (82 ppb) with all remaining PGE totaling to 70 ppb. Again, except for sample C10/959, all chromitites show low Pd/Ir (≤0.10) and Pt + Pd/Ir + Ru ratios (≤0.29); these ratios in C10/959 are higher (4.56 and 1.81, respectively). Gold was detected only in samples with detectable Pt and Pd contents.

When plotted as C1 chondrite-normalized PGE patterns, the Xerolivado-Skoumtsa chromitites display steep but variable positive slopes between Os and Ru, and steep negative slopes between Ru-Pd, the latter owing to enrichment in Ru (Fig. 8a). A few samples define a positive slope in the segments Rh to Pt and Rh to Pd due to enrichment in Pt and Pd (Fig. 8a). The C1 chondrite-normalized PGE profiles of the Xerolivado-Skoumtsa ores fit very well with those of other mantle-hosted ophiolitic chromitites (Fig. 8a), including other chromitite deposits from Greece (Fig. 8b); even though, their major element compositions are quite distinct from those of the Xerolivado-Skoumtsa chromitites. Previous studies of the Xerolivado-Skoumtsa chrome ores show C1

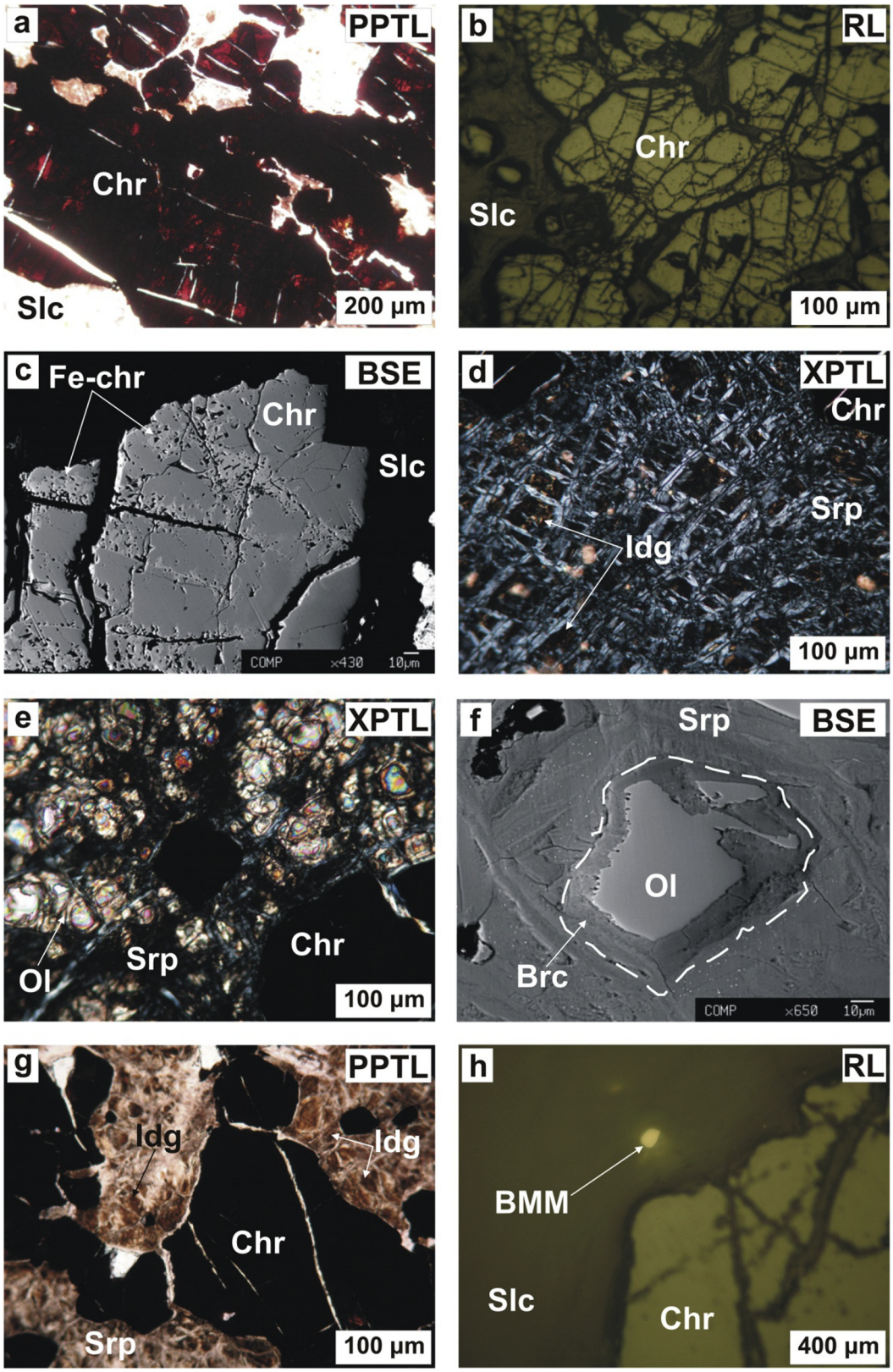

Fig. 5. Photomicrographs of chromitites from the Xerolivado-Skoumtsa locality. a) Dark reddish colored Cr-spinel grains. b) Chromian spinel grains showing cataclastic texture. c) Substitution of Cr-spinel by porous ferrian chromite. d) Complete replacement of interstitial silicate groundmass by serpentine (displaying minor supergene replacement by iddingsite). e) Remnant olivine grains in small clusters surviving pervasive serpentinization. f) Remnant olivine grains surrounded by thin brucite rim. g) Formation of aggregates of brownish iddingsite by supergene alteration/weathering. h) A grain of BMM dispersed in the (serpentinized) silicate matrix of the ores. Abbreviations: Chr – Cr-spinel; Slc – silicates; Fe-chr – ferrian chromite; Srp – serpentine; Idg – iddingsite; Ol – olivine; Brc – brucite; BMM – base metal mineral; PPTL – plane polarized transmitted light; RL – reflected light; XPTL – crossed polarized transmitted light.

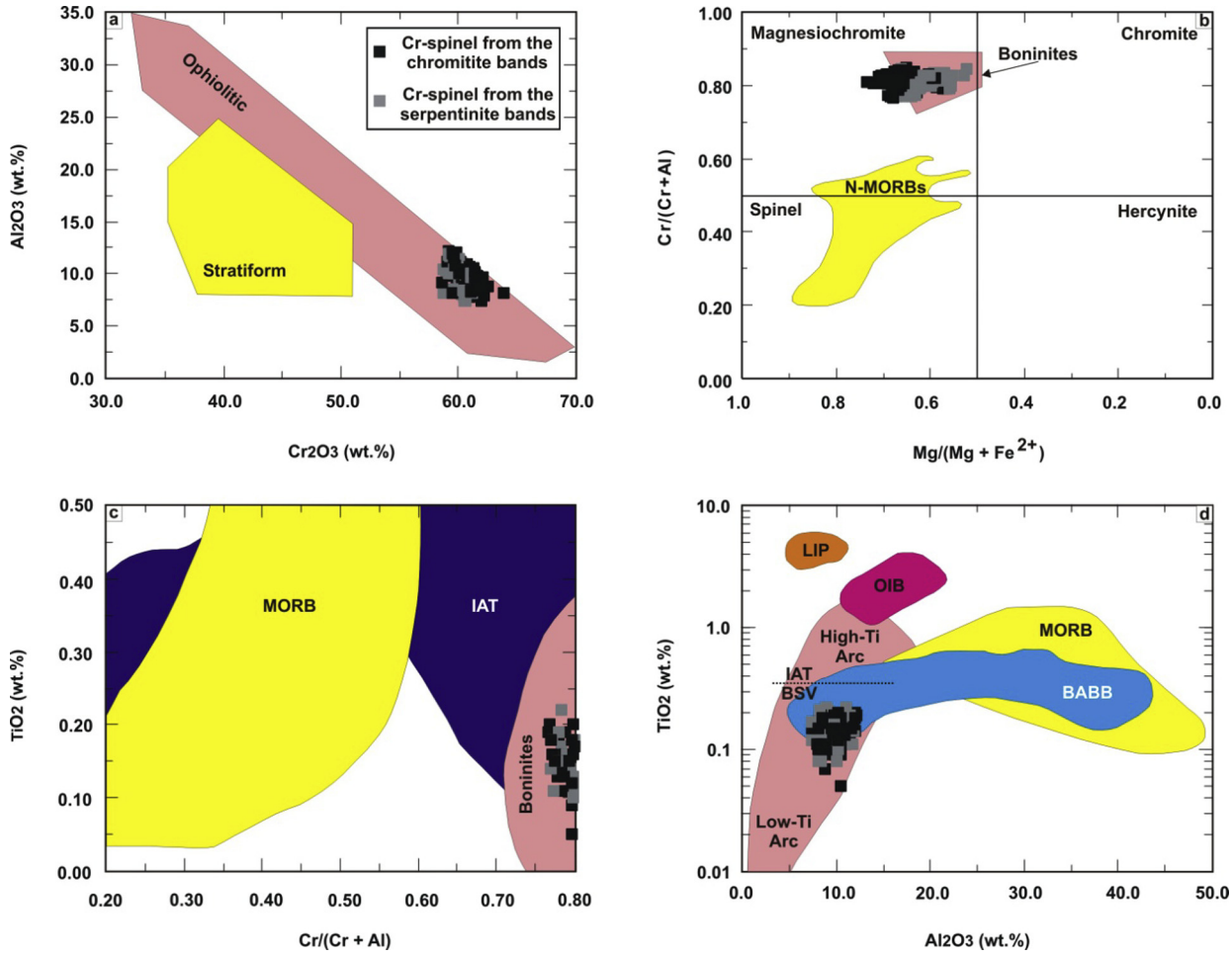

Fig. 6. a) Al_2O_3 (wt%) *vs.* Cr_2O_3 (wt%) variation in Cr-spinels. Fields for podiform and stratiform chromitites are taken from Bonavia et al. (1993). b) Cr/(Cr + Al) *vs.* Mg/(Mg + Fe^{2+}) plot of Cr-spinel from the Xerolivado-Skoumtsa chromitites. Fields for spinel in equilibrium with N-MORBs and boninites are from Dick and Bullen (1984). c) Composition of Cr-spinel from the Xerolivado-Skoumtsa chromitites plotted on the Ti*100 (wt%) *vs.* Cr/(Cr + Al) diagram. All compositional fields are from Arai, 1997b. d) TiO_2 *vs.* Al_2O_3 (wt%) of Cr-spinel from the Xerolivado-Skoumtsa chromitites. Compositional fields are from Kamenetsky et al. (2001). Abbreviations: MORB – mid-ocean ridge basalts; IAT – island arc tholeiites; BSV – boninite series volcanics; OIB – ocean islands basalts; LIP – large igneous province (basalts).

chondrite-normalized PGE patterns characterized by a positive Rh anomaly and almost flat Os-Ru segments (Fig. 8c; Konstantopoulou and Economou-Eliopoulos, 1991; Grammatikopoulos et al., 2011).

8. Discussion

8.1. Deciphering the origin of the Xerolivado-Skoumtsa chromitites

Various models have been proposed to explain chromitite genesis in the oceanic lithospheric mantle. A recent reassessment of these models by González-Jiménez et al. (2014a) led to the petrological assumption that chromitites may be generated by settling of Cr-spinel caused by the mingling of melts of different provenances and SiO_2 contents, at the intersection between high-porosity dunite channels/conduits.

The magmatic processes of origin of the Xerolivado-Skoumtsa chromitites are unsolvable; our geological observations show that these chromitites are polydeformed. The strong imprint of high *T* to relatively low *T* (~1100 °C–700 °C) constrictional deformation in the ductile domain is responsible for their structural layering (Rassios and Dilek, 2009). Field observations indicate that both ore bodies and their surrounding peridotites were trapped into shear zones in lithospheric slab conditions. Within the Xerolivado-Skoumtsa area, the contacts between dunite and harzburgite intra-deformed layers are commonly planar and sharply defined. Dunite layers vary in thickness and 'bifurcate' (via folding and shear deformation); harzburgite generally has blocky foliation next to the dunite layers. Dunite apparently preferentially accommodates strain in these shear zones due to the ease of slip as a result of the nearly monomineralic nature of the rock (Moat, 1986). The thickness and length of the chromitite ore bands do not seem to parallel the morphology of the interlayered dunite bands (Fig. 4a-b), but rather deforms with a different mechanical competency.

Our observations support the idea that the angle between the shear zone and the intersected/entrapped chromitite strongly controls the present image of both ore bodies and host dunites in the study area (Moat, 1986). The obliquity of the shear zone to the initial Cr-spinel concentration was relatively low in the Xerolivado-Skoumtsa host dunite (Fig. 4d), thus allowing shearing to affect the ore body more and more by preferentially propagating through it. With increasing parallelism, the original shape of the ore concentration is obscured: the chromitite obtained a higher Cr-spinel/silicate ratio, a layered form and eventually a strongly foliated structural imprint on the ore layers themselves. We presume that this process would have been (at least in part) responsible for the obliteration of any pre-existing nodular texture in the Xerolivado-Skoumtsa chromitites. Nodular ores are present at

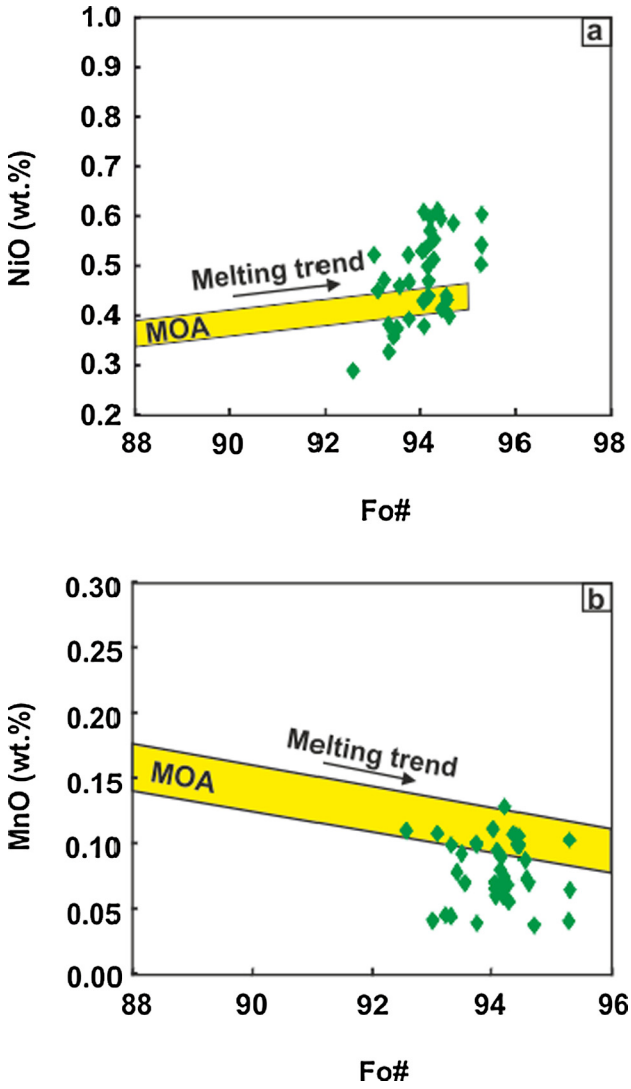

Fig. 7. a) NiO (wt%) and b) MnO (wt%) *vs.* Fo# [100 × Mg/(Mg + Fe^{2+})] of olivine from serpentinite bands (altered dunite) within the Xerolivado-Skoumtsa 'schlieren' ores. Mantle olivine array (MOA) and partial melting trends are from Ozawa (1994).

Vourinos on both sides of the petrological Moho but not at Xerolivado-Skoumtsa (e.g., Rassios et al., 1983).

We must emphasize that the Xerolivado-Skoumtsa ore bodies are part of a metamorphic tectonite complex (Moores, 1969) that has been deformed in plastic (Fig. 4a and d) to ductile (Fig. 4c) and brittle conditions (Fig. 4f, Rassios and Moores, 2006). Studies of this deformation require a strain framework of obduction initiating in near-ridgecrest i.e., ductile conditions. Working back to an original S_0 morphology of these ores is not possible. It is unlikely to determine if they were originally vertical or horizontal, or what comprised their original concentration of Cr-spinel. We conclude that the investigated ore bodies represent metamorphic layers *sensu lato*, (Fig. 4d and e) and not original magmatic layers.

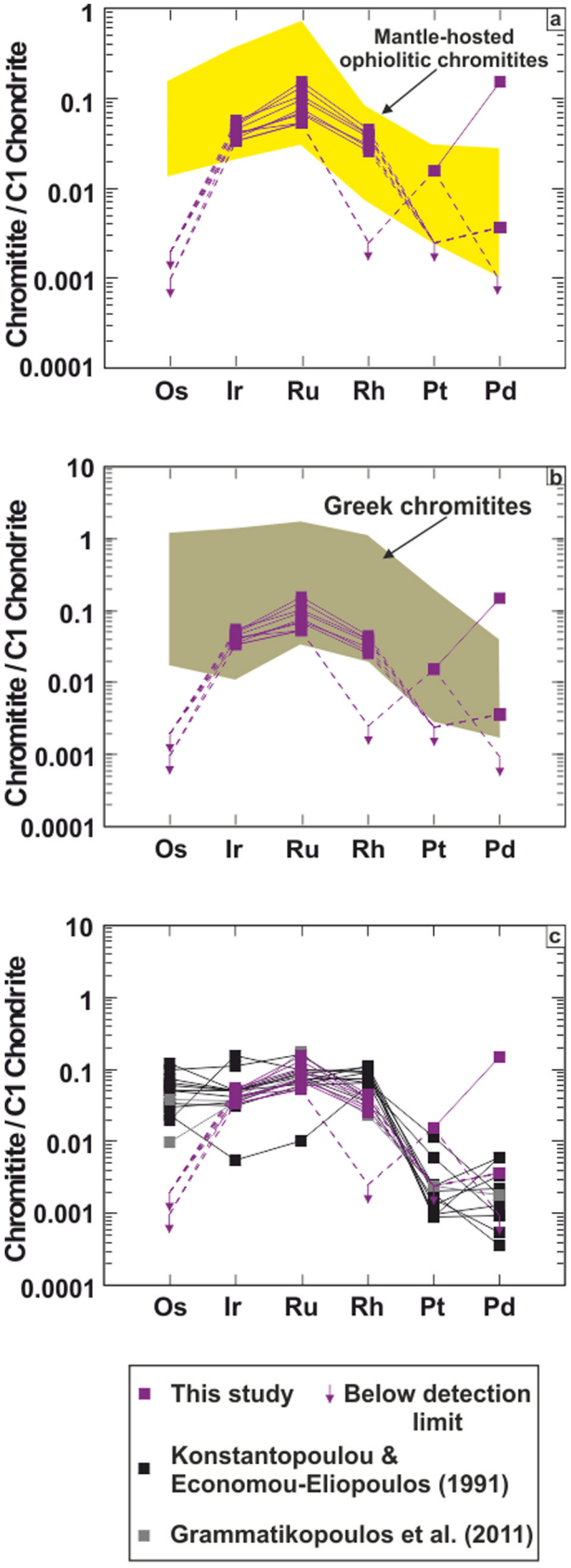

Fig. 8. C1 chondrite-normalized (Naldrett and Duke, 1980) patterns of the Xerolivado-Skoumtsa chromitites and comparison with those from: a) mantle-hosted ophiolitic chromitites from elsewhere (data from Economou-Eliopoulos, 1996; Gauthier et al., 1990; Kojonen et al., 2003; McElduff and Stumpfl, 1990); b) other ophiolitic chromitites from Greece (data from Agiorgitis and Wolf, 1978; Economou-Eliopoulos, 1993; Economou-Eliopoulos and Vacondios, 1995; Konstantopoulou and Economou-Eliopoulos, 1991); c) previous investigations on the Xerolivado-Skoumtsa chromitites (i.e., Grammatikopoulos et al., 2011; Konstantopoulou and Economou-Eliopoulos, 1991).

However, some petrologic 'hints' indicative of the nature of the original magmatic processes remain. For example, the presence of small (0.5–1.0 m), deformed chromitite bodies in proximity to the main ore zones suggests metallogenesis at progressively decreasing melt/rock ratio (e.g., González-Jiménez et al., 2014a), meaning that the major ore layers had a higher melt/rock ratio than elsewhere in the dunite body. These satellite ore bodies may represent late products of spasmodic chromitite formation owing to limited mingling of melts on the margins of dunite channels or penetrations of magma into deforming zones around the chrome ores. The compositional homogeneity shown by Cr-spinel in the Xerolivado-Skoumtsa chromitites may be taken as evidence for their formation in melt flow (however deformed) channels. Furthermore, the compositional homogeneity shown by Cr-spinel in interlayered chromitite and serpentinite bands implies an origin from a common melt (e.g., Arai and Miura, 2016). The high Cr# values and low TiO_2 contents in Cr-spinel from different chromitite bands is unlikely to be due to re-equilibration with olivine or serpentinization owing to the low diffusivity of Cr and Ti (Kamenetsky et al., 2001). Spatial homogeneity must be present within the parental melt composition (as discussed further below). It would seem intuitive that melt-producing processes (that is, the partial melting of the mantle) did not cease instantaneously following the formation of chromitites.

8.2. Chromitite parental melt and geotectonic implications

Chromian spinel is frequently used as a petrogenetic indicator, with its mineral chemistry applied in the determination of the original composition and affinity of the parental melt (e.g., Arai, 1997a; Kamenetsky et al., 2001). However, it is now widely accepted that 'pristine' Cr-spinel chemistry is modified via subsolidus re-equilibration and metamorphic processes (e.g., Barnes, 2000). Subsolidus changes in Cr-spinel compositions are less apparent in massive chromitites than in other textural types of chromitite (e.g., Gervilla et al., 2012). The proportion of Cr-spinel in the chromitite bands investigated in this study is more than 70% modal. According to Tzamos et al. (2016), who studied Cr-spinel-silicate re-equilibration phenomena in the same suite, the substitution of Mg_{Sp} by $Fe^{2+}{}_{Ol}$ appears to be limited in Cr-spinel from the chromitite bands. We analyzed Cr-spinel grains from 'practically monomineralic' and thick chromitite bands (15–20 cm); in addition, the grains were analyzed from the central parts of the bands to best approximate the original magmatic compositions.

Experimental studies of spinel-liquid equilibrium performed at low P (1 bar) by Maurel and Maurel (1982) indicate that the FeO/MgO ratio of the melt in equilibrium with nearly monomineralic chromitites can be computed from Cr-spinel composition using the following formula:

$$\ln(FeO/MgO)_{Cr-spinel} = 0.47 - 1.07Al\#_{Cr-spinel} + 0.64Fe^{3+}\#_{Cr-spinel} + \ln(FeO/MgO)_{melt} \quad (1)$$

where FeO and MgO in wt%, $Al\#_{Cr\text{-}spinel} = Al/(Cr + Al + Fe^{3+})$ and $Fe^{3+}\#_{Cr\text{-}spinel} = Fe^{3+}/(Cr + Al + Fe^{3+})$. The Al_2O_3 content of the melt can be derived from the experimental formula of Maurel and Maurel (1982):

$$(Al_2O_3)_{Cr-spinel} = 0.035(Al_2O_3)^{2.42}_{melt} \quad (2)$$

where Al_2O_3 in wt%. Furthermore, the Al_2O_3 and TiO_2 content of the melt in equilibrium with the high-Cr chromitites from the Xerolivado-Skoumtsa mine can be calculated applying the following logarithmic (/empirical) expressions suggested by Zaccarini et al. (2011):

$$(Al_2O_3)_{melt} = 5.2253\ln(Al_2O_3)_{Cr-spinel} + 1.1232 \quad (3)$$

and

$$(TiO_2)_{melt} = 1.0897(TiO_2)_{Cr-spinel} + 0.0892 \quad (4)$$

The implementation of Eqs. (1) and (2) shows that the parental melt of the Xerolivado-Skoumtsa chromitites had FeO/MgO ratio varying from 0.47 to 1.03 and 9.12 to 11.21 wt% Al_2O_3. The implementation of Eqs. (3) and (4) indicates that the parental melt had 11.55–14.17 wt% Al_2O_3 (Fig. 9a) and 0.15–0.30 wt% TiO_2 (Fig. 9b; Table 5). These results indicate that the composition of the parent melt of the Xerolivado-Skoumtsa chromitites resembles that of high-Mg, low-CaO boninites from the Bonin Island, Japan (Crawford et al., 1989). We note the occurrence of boninite dykes within the upper crustal section of Vourinos (Fig. 2). Similar boninitic melts, but with lower Al_2O_3 and TiO_2 contents and a lower FeO/MgO ratio, have been suggested as responsible for the precipitation of the high-Cr chromitites from Kempirsai in Kazakhstan (Melcher et al., 1997) and in Oman ophiolite (Rollinson, 2008). The parent magmas of the Xerolivado-Skoumtsa chromitites deviate from the Al_2O_3-trend expected for arc melts (Fig. 9a) implying that they could have undergone a limited degree of fractionation at the time of ore mineral precipitation (as indicated by the low Pd/Ir ratio) at lithospheric levels below the petrological Moho.

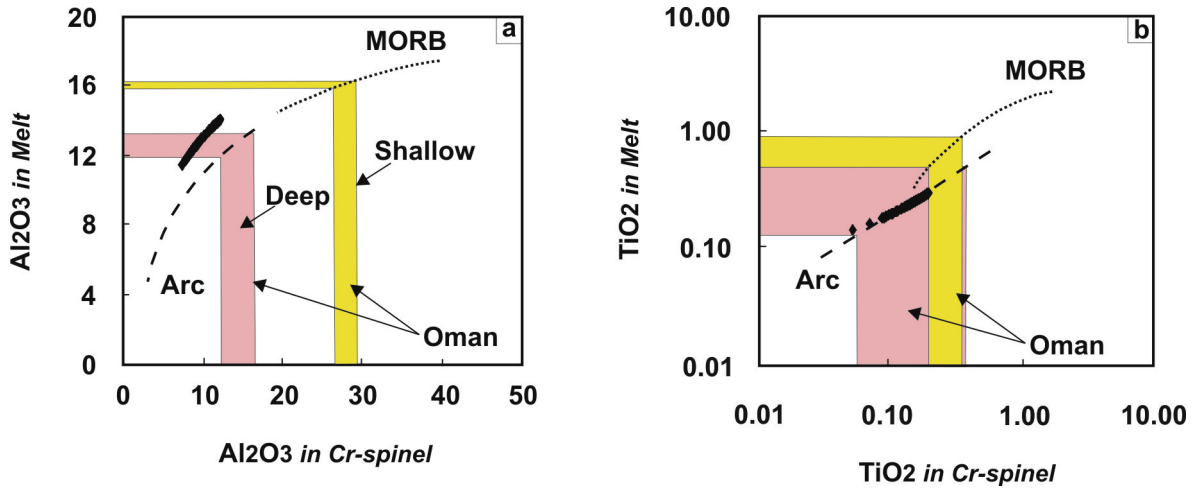

Fig. 9. Plots of Al_2O_3 and TiO_2 calculated to model parental melts in equilibrium with the Xerolivado-Skoumtsa chromitites. The MORB and Arc lines are from Zaccarini et al. (2011). The fields for (deep and shallow) Oman chromitites parental melt composition are from Rollinson (2008).

Table 5
Range of FeO/MgO ratio and Al_2O_3 and TiO_2 (wt%) contents of Cr-spinel in chromitites from the southern sector of the Xerolivado-Skoumtsa Mine and calculated composition of parental melts in equilibrium with chromitites. Computations of FeO/MgO were made using the approach of Maurel and Maurel (1982; Eq. 1), whereas Al_2O_3 and TiO_2 calculations were made applying the equations (Eqs. (3) and (4)) proposed by Zaccarini et al. (2011).

Compositional signatures of parental melts in equilibrium with chromitites							
Study	Area	$Cr\#_{Sp}$	Al_2O_{3Sp}	Al_2O_{3Melt}	TiO_{2Sp}	TiO_{2Melt}	FeO/MgO_{Melt}
Najafzadeh and Ahmadipour (2014)	Soghan mafic-ultramafic complex		9.30	10.57	0.18	0.28	0.74
González-Jiménez et al. (2011)	Sagua de Tanamo(Eastern Cuba)	0.63–0.72	16.28	13.42	0.19	0.30	
Rollinson (2008)	Oman	0.71–0.77	11.7–14.4	11.80–12.90		0.23–0.34	
Melcher et al. (1997)	Kempirsai (Kazakhstan)			9.00–10.60			0.30–0.50
Zaccarini et al. (2011)	Santa Elena nappe (Costa Rica)	0.81	10.30–17.50	11.2–13.0	0.14–0.20	0.28–0.38	
This study	Xerolivado-Skoumtsa mine	0.77–0.85	7.36–12.14	11.55–14.17	0.05–0.20	0.15–0.30	0.47–1.03
Wilson (1989)	Boninite			10.60–14.40		0.25	0.70–1.40
Wilson (1989)	MORB			~15.00			1.20–1.60

The presence of pargasite inclusions in Cr-spinel grains within the Xerolivado-Skoumtsa ore bodies provides indirect evidence for the existence of alkali-bearing, hydrous parental melts (e.g., Johan et al., 1983). The scarcity of igneous sulfides in these ores and their low Pt + Pd/Ir + Ru ratios indicate that they crystallized from S-undersaturated melts that had experienced limited fractionation. Boninite magmas are known to be S-undersaturated (Keays, 1995) and to be generated by fluid-assisted melting of a depleted mantle source (Hamlyn and Keays, 1986) beneath the forearc region of a SSZ (e.g., Crawford et al., 1989).

As subduction processes continue and the undergoing lithospheric slab is translated to greater and hotter depths, the volume of hydrous fluids emanating from its top increases (Fig. 10a): such a process could stimulate optimal conditions for melting and subsequent peridotite-melt interaction in the overlying previously depleted, lithospheric mantle (Fig. 10b and c; e.g., Derbyshire et al., 2013). Ophiolitic chromitites form mainly in settings of harzburgite-melt interaction (Fig. 10c; e.g., Zhou et al., 1996). Their precipitation depends on the silica content of partial melts migrating through the mantle and the opportunity these melts have to mix (Fig. 10b and c). The character of these melts depends on: i) the composition and degree of partial melting of the mantle source, and ii) further mantle orthopyroxene dissolution during harzburgite-melt interaction (e.g., Arai and Yurimoto, 1994). During both phases, orthopyroxene provides an important source of silica and Cr to the migrating melts. However, during harzburgite-melt interaction orthopyroxene dissolution promotes harzburgite replacement by (high-porosity) dunite along the interaction wall (Fig. 10c). Multiple intrusions of primitive olivine-saturated melts and their mixing with the more evolved melts within dunite (Lago et al., 1982) is one proposed method for decreasing Cr solubility, thereby triggering Cr-spinel precipitation and subsequently the formation of chromitites (Fig. 10c; e.g., González-Jiménez et al., 2014a). The close association between dunite (serpentinite) and chromitites in Xerolivado-Skoumtsa, though now structurally controlled, is evidence for the original coeval formation of dunite and chromitite.

The high chrome content of the Xerolivado-Skoumtsa chromitites would be facilitated by parental melts generated during an advanced stage of slab dehydration (Fig. 10a). Elsewhere in Vourinos (i.e., Voidolakkos) the existence of late hydrous mantle melts and addition of slab-derived components such as water and LREE has been documented (Saccani et al., 2011; Kapsiotis, 2013). Numerical modelling suggests that up to 30% melting of an originally fertile mantle source via cumulative melting, and enrichment in SSZ-derived components, would be needed to produce the boninitic chemistries found in the Mesohellenic ophiolites (Saccani et al., 2004). The low Al content of the Xerolivado-Skoumtsa ores and the presence of hydrous silicate inclusions suggest their formation from melts above a subduction zone (e.g., as suggested by Khedr and Arai, 2016). As subduction continues, partial melting and magma generation would wane beneath the forearc region. Possibly, undeformed pyroxenite pegmatite dykes cross-cutting the Vourinos lithosphere represent the 'last gasp' of this magmatism (Rassios and Dilek, 2009). Arc-type, boninitic affinity intrusions (Kapsiotis, 2016) contradict the possibility of interaction between the asthenospheric material and the depleted mantle after the formation of high-Cr chromitites (e.g., Khedr and Arai, 2016). As we have suggested, the metallogenesis of these chromitites necessitates a hydrated mantle beneath the forearc, a region which is petrologically/thermally 'isolated' from intense asthenospheric upwelling (e.g., Bostock et al., 2002).

8.3. Controls on PGE distribution

The content of PGE in ophiolitic chromitites is controlled by three processes; partial melting, magma fractionation and hydrothermal alteration (e.g., Barnes et al., 1985; Najafzadeh and Ahmadipour, 2014). The Xerolivado-Skoumtsa chromitites are enriched in IPGE over PPGE as is typical for chromitites hosted in the mantle section of ophiolites (e.g., Gauthier et al., 1990; Kojonen et al., 2003). The selective incorporation of Ru and Ir in these ores (Table 4) demonstrates the capability of Cr-spinel in concentrating these metals, that is, by promoting local saturation of the parental melts of chromitites in these two easily oxidized noble elements (e.g., Finnigan et al., 2008). This can be explained by the preferential partition of Al^{3+}, Cr^{3+} and Fe^{3+} into the Cr-spinel lattice that will lead to the formation of a 'reduced zone' at the edges of the growing Cr-spinel crystals. This will cause saturation of Ir and Ru in the Cr-spinel-melt boundary layer and both metals will eventually be fractionated along with Cr-spinel (e.g., Ballhaus et al., 2006). It has also been suggested that the distribution of Ir and Ru in ophiolitic chromitites could be related to 'nugget' effects synchronous to the (early) igneous crystallization of platinum-group minerals (PGM); this 'nugget' effect model has been proposed in older studies of the Xerolivado-Skoumtsa chromitites (Grammatikopoulos et al., 2011).

The similar C1 chondrite-normalized PGE patterns of the Xerolivado-Skoumtsa chrome ores (Fig. 8a) implies that their PGE budgets were controlled by one single petrological process, or by a combination of petrological processes that similarly affected all ores. These chromitites have 'customarily' been considered as compositionally homogeneous in terms of the total PGE abundance (Konstantopoulou and Economou-Eliopoulos, 1991). Our data, however, show noteworthy variation in Ru concentration (36 up to 105 ppb) over almost constant $Cr\#_{Sp}$ values (77–85). If we consider that these chromitites crystallized from a single boninitic melt (Grammatikopoulos et al., 2011), then Ru concentration would be expected to decrease with decreasing $Cr\#_{Sp}$ values. This is not the case. Instead we propose that our documented variation

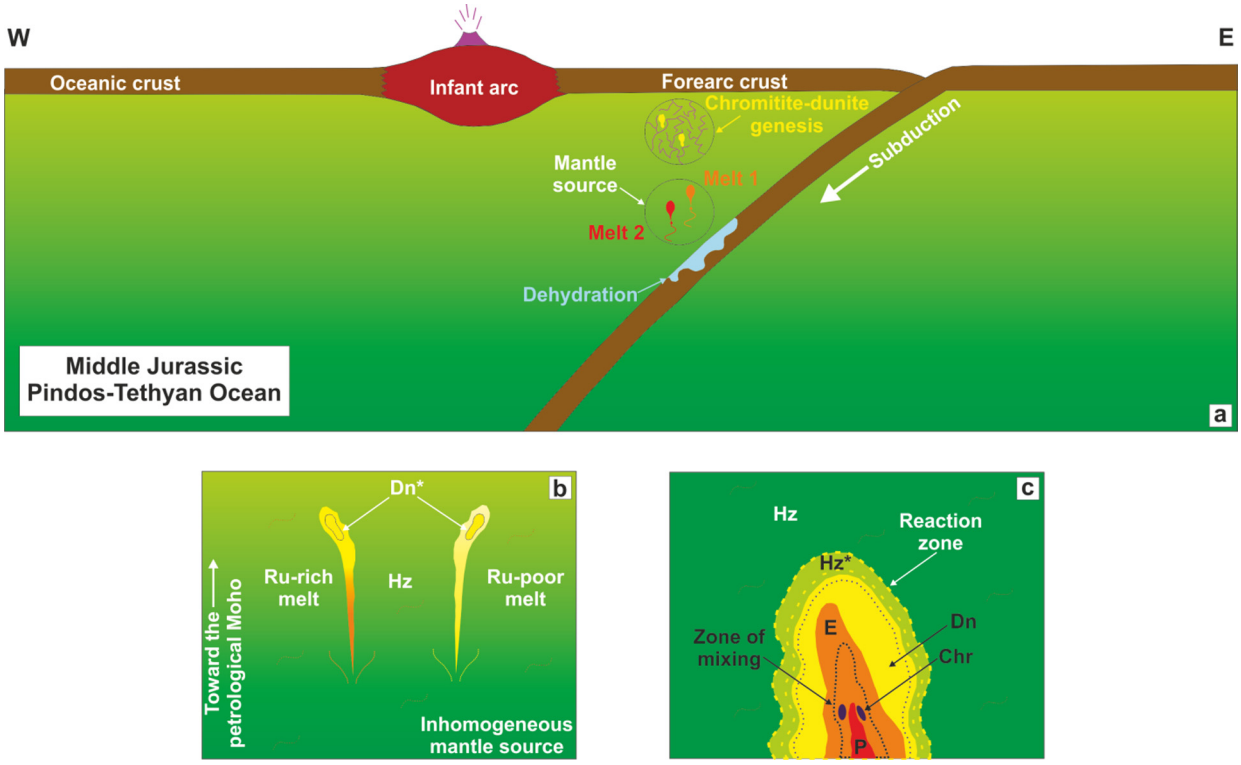

Fig. 10. a) Schematic cartoon illustrating the geotectonic setting of the Xerolivado-Skoumtsa high-Cr chromitites. b) Ore precipitation at the same mantle level from distinct magmas derived from melting of an inhomogeneous (in terms of PGE and especially Ru content) mantle source region. c) Formation of dunite with chromitite pods in the upper mantle. Mantle harzburgite is metasomatically replaced by dunite. Chromitites are formed from hybridized melts generated by mixing of evolved melts and primitive melts within the same magma conduit. Foliation is shown by dotted wavy red lines. Abbreviations: Chr – chromitite; Dn – dunite; Dn* – dunite hosting chromitites; E – evolved melt; Hz – harzburgite; Hz* – harzburgite with low orthopyroxene content; P – primitive melt.

in Ru is due to an inherited variation present in their immediate parental melt; these chromitites do not represent a homogeneous group of ore bodies that precipitated from a progressively differentiating boninitic melt (Grammatikopoulos et al., 2011), but they do have a rather 'polygenetic' origin attributed to metallogenesis from distinct boninitic melt inputs; each melt input originates in the same SSZ environment, but derives from different sections of the upper mantle (Fig. 10a-b). The Vourinos upper mantle itself, re-melted at various stages during a long lithospheric history, and was inhomogeneous in terms of PGE content (Grammatikopoulos et al., 2011). The relatively broad range of Ru concentration may be due to heterogeneous distribution of Ru-rich minerals in the Vourinos depleted mantle suite at a micron scale (see chapter 8.4). The inhomogeneous distribution of these microphases may cause extreme nugget effects, such as those documented in the C1 chondrite-normalized PGE patterns of the examined chromitites (i.e., positive Ru anomalies; Fig. 8a).

Some analyses of our chromitite samples are relatively high in Pt + Pd/Ir + Ru ratios (>0.27), and show C1 chondrite-normalized PGE patterns with positive slopes in the Rh to Pt and Rh to Pd segments (Fig. 8a). This pattern appears exceptional among ophiolitic chromitites as their C1 chondrite-normalized PGE profiles are commonly characterized by negatively sloping Ru to Pd segments (e.g., Economou-Eliopoulos, 1996; Gervilla et al., 2005). This exceptional slope for the Xerolivado-Skoumtsa ores must be a result of the remobilization and reconcentration of Pd and Pt during the post-magmatic stage of evolution. The absence of igneous base metal sulfides (BMS), as well as Pt- and/or Pd-dominant primary minerals from the South Vourinos chromitites (Augé, 1985; Garuti and Zaccarini, 1997; Grammatikopoulos et al., 2011), leads us to believe that both Pt and Pd were incorporated in the lattice of hydrothermally precipitated PGM (Garuti and Zaccarini, 1997). Gold was only detected in Pd- and Pt-rich chromitite samples, and is also presumed to be derived in the post-magmatic period.

We conclude that the bulk-rock PGE content in the Xerolivado-Skoumtsa ore samples is generally magmatic in origin; occasional mineralization at lower (hydrothermal) *T* processes had a limited effect on concentrations of Pt and Pd and did not modify the magmatic distribution of Ir, Ru and Rh.

8.4. PGE-signature inheritance from a depleted mantle source

The Xerolivado-Skoumtsa chromitites are enriched in Ir and Ru compared to the less refractory PPGE. However, this intragroup fractionation cannot be simply explained by the incompatible behavior of the PPGE compared to the IPGE during mantle melting (Barnes et al., 1985). Neither Pt- nor Pd-based primary minerals have been found in the mantle chromitites of Vourinos (Augé, 1985; Garuti and Zaccarini, 1997; Grammatikopoulos et al., 2011); which lead to the question as to whether the vast majority of PPGE were removed from the Vourinos mantle by the time the chromitites formed.

Platinum-group metals behave as chalcophile elements during mantle melting; they are hosted in accessory Cu-Fe-Ni sulfides in mantle peridotites (e.g., Keays, 1995). Low degrees of partial melting (<20%; i.e., at MOR) produce PGE-poor melts by removing Pd ± Pt-Cu-Ni-rich sulfides, and leaving behind a residual IPGE-bearing monosulfide solid solution (*Mss*). The formation of IPGE-rich melts, similar to those that formed the chromitites in this study, appears to support at higher degrees (20–25%) of mantle melting (such as those in SSZ). At such high degrees of mantle melting the IPGE will be liberated to the melt and the residual *Mss.* will decompose into Ru-Os-Ir refractory PGM (alloys, sulfides)

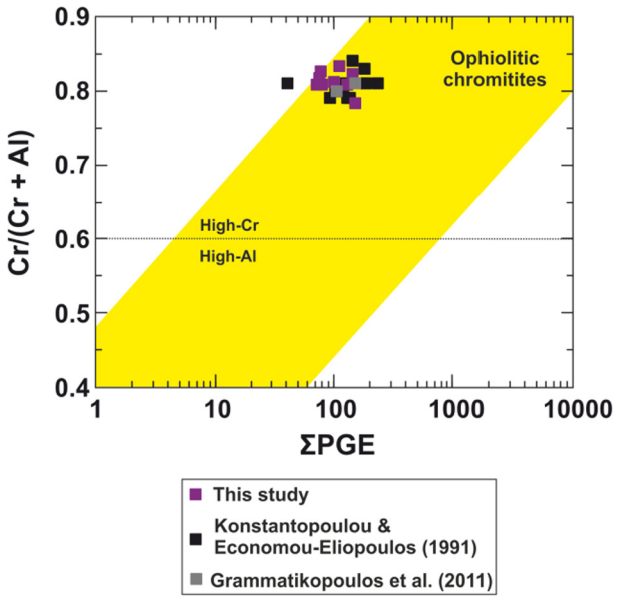

Fig. 11. Cr/(Cr + Al) *vs.* bulk PGE content in the chromitites and comparison with mantle-hosted ophiolitic chromitites from elsewhere. Data sources: Moa-Baracoa and Mayarí, Eastern Cuba (Gervilla et al., 2005; Proenza et al., 1999), Greek ophiolites (Othris, Rodiani, Vourinos, Kissavos, Pindos, Thessaly, Vermio, Veria, Edessa; Economou-Eliopoulos, 1996; Konstantopoulou and Economou-Eliopoulos, 1991), Serbian ophiolites (Radusa, Brecovitsa, Veluce; Economou-Eliopoulos, 1996), Oman (Ahmed and Arai, 2002), Luobusa (Zhou et al., 1996).

as the partial melts become S-undersaturated (e.g., O'Driscoll and González-Jiménez, 2016 and references therein).

The modeling of partial melting in Vourinos indicates that the harzburgite hosts represent mantle residues after 26–27% cumulative melting of a primitive mantle (PM) source in two different geotectonic regimes (Kapsiotis, 2016). This melting was efficient, so that a critical phase of PGE extraction occurred as PGE-bearing minerals were largely removed from the Vourinos multi-depleted mantle suite (e.g., Konstantopoulou, 1990). We therefore believe that tiny grains of IPGE-rich *Mss* and alloys were the dominant PGE-mineral carriers in the Vourinos depleted mantle during the melting episode that produced the parental melts of chromitites in the mantle wedge above a SSZ. This fluid-assisted, second-stage melting episode caused drastic dissolution of the IPGE-bearing particles, which in turn triggered almost complete removal of Ir, Ru and any PPGE left from the mantle. Furthermore, this melting episode was strong enough to cause dilution of Pt and Pd in the resultant Ir- and Ru-rich melts parental to chromitites (e.g., Prichard et al., 2008). The formation of PPGE-poor, IPGE-rich chromitites is commonly linked to high degrees of partial melting (20–25%) leading to almost complete dissolution of PGE-mineral carriers from the mantle (e.g., González-Jiménez et al., 2011).

The harzburgite tectonites of Vourinos lack significant quantities of primary mantle or metasomatically-added sulfides (Kapsiotis, 2009), and are in general PGE-poor (Konstantopoulou, 1990), because they were strongly depleted in these elements by the time of the origin of boninitic melts. Boninites are normally high in PGE elements (Keays, 1995), and any 'daughter' chromitites precipitated from boninitic magmas would be expected to have similarly high PGE contents. Vourinos is a lithospheric complex possessing a great affinity for boninitic activity. Its lack of significant levels of PGE in chromitites appears an intrinsic feature inherited from its primary mantle source, not from boninite-harzburgite interaction. There is no correlation between the Cr# of Cr-spinel and the PGE abundance within Xerolivado-Skoumtsa chromitites (e.g., González-Jiménez et al., 2011; Fig. 11). This means that the PGE budget of the Xerolivado-Skoumtsa chromitites was not acquired via the interaction of migrating boninitic melts with the harzburgites encountered *en route* to shallow (chrome ore hosting) mantle levels. The consistently impoverished nature of the Vourinos restitic harzburgite (Konstantopoulou, 1990) reflects the PGE budget of the parental melts of the investigated chromitites, and by extension, the PGE content of the previously melted, deep mantle (sub forearc) source region of these magmas.

9. Concluding remarks

1. Field observations demonstrate that the schlieren texture and banded morphology of the Xerolivado-Skoumtsa chromitites are artifacts of tectonometamorphism acquired during a complex history of ductile shearing and folding (post crystallization).
2. The Xerolivado-Skoumtsa ore bodies are high-Cr (Cr_{Sp}# = 0.77-0.85) and relatively enriched in Ir and Ru, implying that they crystallized from S-undersaturated, hydrous boninitic melts within a mantle wedge beneath a forearc basin at an advanced stage of lithospheric subduction.
3. Ruthenium concentrations in the ores are variable, but $Cr\#_{Sp}$ is constant. This indicates that the PGE-signature of the Xerolivado-Skoumtsa chromitites is an intrinsic and identifying feature of the heterogeneously depleted mantle source of their parental melts.

Acknowledgements

A. Risplendente from the University of Milan is acknowledged for his assistance at the stage of electron micro-probe analyses. K. Stamoulis is also thanked for providing photos and aiding in samples collection. We are grateful to the Guest Editor Dr. R. Mukherjee and to Drs. G. Garuti and P. Voudouris for their constructive feedback, which greatly improved our manuscript. E. Tzamos would like to express his gratitude to the Greek State Scholarship Foundation (IKY) for partially financing his Ph.D. research, part of which is presented in this paper. Part of this research was also supported by a Youth Science Fund Project (No. 41402065) awarded from the National Natural Science Foundation of China (NNSFC) to A. Kapsiotis.

References

Agiorgitis, G., Wolf, R., 1978. Aspects of osmium, ruthenium and iridium contents in some Greek chromites. Chem. Geol. 23, 267–272.
Ahmed, A.H., Arai, S., 2002. Unexpectedly high-PGE chromitite from the deeper mantle section of the northern Oman ophiolite and its tectonic implications. Contrib. Min. Petrol. 143, 263–278.
Anonymous, 1972. Penrose field conference on ophiolites. Geotimes 17 (12), 24–25.
Arai, S., 1997a. Origin of podiform chromitites. J. Asian Earth Sci. 15, 303–310.
Arai, S., 1997b. Control of wall-rock composition on the formation of podiform chromitites as a result of magma/peridotite interaction. Res. Geol. 47, 177–187.
Arai, S., Miura, M., 2016. Formation and modification of chromitites in the mantle. Lithos 264, 277–295.
Arai, S., Yurimoto, H., 1994. Podiform chromitites of the Tari-Misaka ultramafic complex, Southwest Japan, as mantle–melt interaction products. Econ. Geol. 89, 1279–1288.
Arai, S., Yurimoto, H., 1995. Possible sub-arc origin of podiform chromitites. The Isl. Arc 4, 104–111.
Augé, T., 1985. Platinum-group mineral inclusions in ophiolitic chromitite from the Vourinos Complex, Greece. Can. Min. 23, 163–171.
Ballhaus, C., Bockrath, C., Wohlegemuth-Uberwasser, C., Laurenz, V., Berndt, J., 2006. Fractionation of the noble metals by physical processes. Contrib. Min. Petrol. 152, 667–684.
Barnes, S.J., 2000. Chromite in Komatiites, II. Modification during greenschist to mid-amphibolite facies metamorphism. J. Petrol. 41, 387–409.
Barnes, S.J., Naldrett, A.J., Gorton, M.P., 1985. The origin of the fractionation of the platinum-group elements in terrestrial magmas. Chem. Geol. 53, 303–323.
Bonavia, F.F., Diella, V., Ferrario, A., 1993. Precambrian podiform chromitites from Kenticha Hill, Southern Ethiopia. Econ. Geol. 88, 198–202.

Bostock, M.G., Hyndman, R.D., Rondenay, S., Peacockk, S.M., 2002. An inverted continental Moho and serpentinization of the fore-arc mantle. Let. Nature 417, 536–538.
Crawford, A.J., Falloon, T.J., Green, D.H., 1989. Classification, petrogenesis and tectonic setting of boninites. In: Crawford, A.J. (Ed.), Boninites and Related Rocks. Unwin Hyman, London, U.K., pp. 1–49.
Derbyshire, E.J., O'Driscoll, B., Lenaz, D., Gertisser, R., Kronz, A., 2013. Compositionally heterogeneous podiform chromitite in the Shetland Ophiolite Complex (Scotland): implications for chromitite petrogenesis and late-stage alteration in the upper mantle portion of a supra-subduction zone ophiolite. Lithos 162–163, 279–300.
Dick, H.J.B., Bullen, T., 1984. Chromian spinel as a petrogenetic indicator in abyssal and alpine-type peridotites and spatially associated lavas. Contrib. Min. Petrol. 86, 54–76.
Economou-Eliopoulos, M., 1993. Platinum-group element (PGE) distribution in chromite ores from ophiolite complexes of Greece: implications for chromite exploration. Ofiol 18, 83–97.
Economou-Eliopoulos, M., 1996. Platinum-group element distribution in chromite ores from ophiolite complexes: implications for their exploration. Ore Geol. Rev. 11, 363–381.
Economou-Eliopoulos, M., Vacondios, I., 1995. Geochemistry of chromitites and host rocks from the Pindos ophiolite complex, Greece. Chem. Geol. 122, 99–108.
Finnigan, C.S., Brenan, J.M., Mungall, J.E., McDonough, W.F., 2008. Experiments and models bearing on the role of chromite as a collector of platinum group minerals by local reduction. J. Petrol. 49, 1647–1665.
Garuti, G., Zaccarini, F., 1997. *In situ* alteration of platinum-group minerals at low temperature: evidence from serpentinized and weathered chromitite of the Vourinos Complex, Greece. Can. Min. 35, 611–626.
Gauthier, M., Corrivaux, L., Trottier, L.J., Laflamme, G.J.H., Bergerson, M., 1990. Chromitites platinifères des complexes ophiolitiques de l' Estrie-Beauce, Appalaches du Sud du Quebec. Miner. Dep. 25, 169–178.
Gervilla, F., Proenza, J.A., Frei, R., González-Jiménez, J.M., Garrido, C.J., Melgarejo, J.C., Meibom, A., Díaz-Martínez, R., Lavaut, W., 2005. Distribution of platinum-group elements and Os isotopes in chromite ores from Mayarí-Baracoa Ophiolite Belt (eastern Cuba). Contrib. Min. Petrol. 150, 589–607.
Gervilla, F., Padrón-Navarta, J.A., Kerestedjian, T., Sergeeva, I., González-Jiménez, J. M., Fanlo, I., 2012. Formation of ferrian chromite in podiform chromitites from the Golyamo Kamenyane serpentinite, Eastern Rhodopes, SE Bulgaria: a two-stage process. Contrib. Min. Petrol. 164 (4), 643–657.
Ghikas, C., Dilek, Y., Rassios, A., 2010. Structure and tectonics of subophiolitic mélanges in the western Hellenides (Greece): implications for ophiolite emplacement tectonics. Inter. Geol. Rev. 52 (4–6), 423–453.
González-Jiménez, J.M., Proenza, J.A., Gervilla, F., Melgarejo, J.C., Blanco-Moreno, J. A., Ruiz-, Sánchez R., Griffin, W.L., 2011. High-Cr and high-Al chromitites from the Sagua de Tánamo district, Mayarí-Cristal Ophiolitic Massif (eastern Cuba): constraints on their origin from mineralogy and geochemistry of chromian spinel and platinum-group elements. Lithos 125, 101–121.
González-Jiménez, J.M., Griffin, W.L., Proenza, J.A., Gervilla, F., O'Reilly, S.Y., Akbulut, M., Pearson, N.J., Arai, S., 2014a. Chromitites in ophiolites: how, where, when, why? Part II. The crystallization of chromitites. Lithos 189, 140–158.
González-Jiménez, J.M., Griffin, W.L., Gervilla, F., Proenza, J.A., O'Reilly, S.Y., Pearson, N.J., 2014b. Chromitites in ophiolites: how, where, when, why? Part I. Origin and significance of platinum-group minerals. Lithos 189, 127–139.
Grammatikopoulos, T.A., Kapsiotis, A., Tsikouras, B., Hatzipanagiotou, K., Zaccarini, F., Garuti, G., 2011. Spinel composition, PGE geochemistry and mineralogy of the chromitites from the Vourinos ophiolite complex, northwestern Greece. Can. Min. 49, 1571–1598.
Grieco, G., Merlini, A., 2012. Chromite alteration processes within Vourinos ophiolite. Int. J. Earth Sci. 101 (6), 1523–1533.
Grivas, E., Rassios, A., Konstantopoulou, G., Vacondios, I., Vrahatis, G., 1993. Drilling for "blind" podiform chrome ore bodies at Voidolakkos in the Vourinos ophiolite complex, Greece. Econ. Geol. 88, 461–468.
Grivas, E., Roberts, S., Vrahatis, S., 1986. Structural geology of the Xerolivado Ore District. In: Rassios, A., Roberts, S., Vacondios, I. (Eds.), The application of a multidisciplinary concept for chromite exploration in the vourinos complex (N. Greece), 409. Institute of Geology and Mineral Exploration, Athens, pp. 217–231.
Hamlyn, P.R., Keays, R.R., 1986. Sulphur saturation and second-stage melts: application to the Bushveld platinum metal deposits. Econ. Geol. 81, 1431–1445.
Jackson, E.D., Green, H.W., Moores, E.M., 1975. The Vourinos ophiolite, Greece: cyclic unit of lineated cumulates overlying harzburgite tectonite. GSA Bull. 86, 390–398.
Johan, Z., Dunlop, H., Le Bel, L., Robert, J.L., Volfinger, M., 1983. Origin of chromite deposits in ophiolitic complexes: evidence for a volatile and Na-rich reducing fluid. Fortschr. Mineral. 61, 105–107.
Kamenetsky, V.S., Crawford, A.J., Meffre, S., 2001. Factors controlling chemistry of magmatic spinel: an empirical study of associated olivine, Cr-spinel and melt inclusions from primitive rocks. J. Petrol. 42, 655–671.
Kapsiotis, A., 2009. PGM and chromite mineralization associated with the petrogenesis of the Vourinos and Pindos Ophiolite Complexes, northwestern Greece (Unpublished Ph.D. Thesis). University of Patras, Patras, Greece, pp. 1–891.
Kapsiotis, A., 2013. Origin of mantle peridotites from the Vourinos Ophiolite Complex, Greece, as deduced from Cr-spinel morphological and chemical variations. J. Geosci. 58, 221–235.
Kapsiotis, A., 2015. Alteration of chromitites from Voidolakkos and Xerolivado mines, Vourinos ophiolite complex, Greece: implications for deformation-induced metamorphism. Geol. J. 50 (6), 739–763.
Kapsiotis, A., 2016. Physiognomy and timing of metasomatism in the southern Vourinos ultramafic suite, NW Greece: a chronicle of consecutive episodes of melt extraction and stagnation in the Neotethyan lithospheric mantle. Int. J. Earth Sci. 105, 983–1013.
Kapsiotis, A., Grammatikopoulos, T.A., Zaccarini, F., Tsikouras, B., Hatzipanagiotou, K., Garuti, G., 2009. Chromian spinel composition and platinum-group element (PGE) mineralogy of the chromitites from Milia area, Pindos ophiolite complex (NW Greece). Can. Min. 47, 1037–1056.
Keays, R.R., 1995. The role of komatiitic magmatism and S-saturation in the formation of ore deposits. Lithos 34, 1–18.
Khedr, M.Z., Arai, S., 2016. Chemical variations of mineral inclusions in Neoproterozoic high-Cr chromitites from Egypt: evidence of fluids during chromitite genesis. Lithos 240–243, 309–326.
Kojonen, K., Zaccarini, F., Garuti, G., 2003. Platinum-group elements and gold geochemistry and mineralogy in the Ray-Iz ophiolitic chromitites, Polar Urals. In: Eliopoulos, D.G. et al. (Eds.), Mineral Exploration and Sustainable Development. Mill Press, Rotterdam, The Netherlands, pp. 599–602.
Konstantopoulou, G.P., 1990. Distribution of platinum-group elements and gold in chromite ores and host rocks of the Vourinos ophiolite complex (Unpublished Ph.D. Thesis). University of Athens, Athens, Greece, pp. 1-272.
Konstantopoulou, G., Economou-Eliopoulos, M., 1991. Distribution of platinum-group elements and gold within the Vourinos chromitite ores, Greece. Econ. Geol. 86, 1672–1682.
Lago, B.L., Rabinowicz, M., Nicolas, A., 1982. Podiform chromitite ore bodies: a genetic model. J. Petrol. 23, 103–125.
Leblanc, M., Nicolas, A., 1992. Ophiolitic chromitites. Int. Geol. Rev. 34, 653–686.
Liati, A., Gebauer, D., Fanning, M., 2004. The age of ophiolitic rocks of the Hellenides Vourinos, Pindos, Crete): first U-Pb ion microprobe (SHRIMP) zircon ages. Chem. Geol. 207, 171–188.
Matveev, S., Ballhaus, C., 2002. Role of water in the origin of podiform chromitite deposits. Earth Planet. Sci. Lett. 203, 235–243.
Maurel, C., Maurel, P., 1982. Étude expérimentale de la distribution de l'aluminium entre bain silicaté basique et spinelle chromifère. Implications pétrogénétiques: teneur en chrome des spinelles. Bull. Min. 105, 197–202.
McElduff, B., Stumpfl, E.F., 1990. Platinum-group minerals from the Troodos ophiolite, Cyprus. Min. Petrol. 42, 211–232.
Melcher, F., Grum, W., Simon, G., Thalhammer, T.V., Stumpfl, E.F., 1997. Petrogenesis of the ophiolitic giant chromite deposits of Kempirsai, Kazakhstan: a study of solid and fluid inclusions in chromite. J. Petrol. 38, 1419–1458.
Moat, T., 1986. Appendix IX. Microfabric and Rock Deformation Studies: Competency contrast and its control on structural behavior of mixed lithological sequences. In: Rassios, A., Roberts, S., Vacondios, I. (Eds.), The Application of a Multidisciplinary Concept for Chromite Exploration in the Vourinos Complex (N. Greece). Institute of Geology and Mineral Exploration, Athens, pp. 284–290.
Moores, E.M., 1969. Petrology and structure of the Vourinos ophiolite complex of Northern Greece. Geol. Soc. Am. Spec. Pap. 118, 1–74.
Naldrett, A.J., Duke, J.M., 1980. Pt metals in magmatic sulfide ores. Science 208, 1417–1424.
Najafzadeh, A.R., Ahmadipour, H., 2014. Using platinum-group elements and Au geochemistry to constrain the genesis of podiform chromitites and associated peridotites from the Soghan mafic-ultramafic complex, Kerman, Southeastern Iran. Ore Geol. Rev. 60, 60–75.
O'Driscoll, B., González-Jiménez, J.M., 2016. Petrogenesis of the Platinum-group Minerals (PGM). Rev. Min. Geochem. 81, 489–578.
O'Hara, M.J., Fry, N., Prichard, H.M., 2001. Minor phases as carriers of trace elements in non-modal crystal liquid separation processes, II: Illustrations and bearing on behavior of REE, U, Th and PGE in igneous processes. J. Petrol. 42, 1887–1910.
Ozawa, K., 1994. Melting and melt segregation in the mantle wedge above a subduction zone: Evidence from the chromitite-bearing peridotites of the Miyamori ophiolite complex, northeastern Japan. J. Petrol. 25, 647–678.
Pagé, P., Barnes, S.-J., 2009. Using trace-elements in chromites to constrain the origin of podiform chromitites in the Thetford Mines Ophiolite, Québec, Canada. Econ. Geol. 104, 997–1018.
Prichard, H.M., Neary, C.R., Fisher, F.C., O'Hara, M.J., 2008. PGE-rich Podiform chromitites in the Al'Ays ophiolite complex, Saudi Arabia: an example of critical mantle melting to extract and concentrate PGE. Econ. Geol. 103, 1507–1529.
Proenza, J.A., Gervilla, F., Melgarejo, J.C., Bodinier, J.L., 1999. Al- and Cr-rich chromitites from the Mayarí-Baracoa ophiolitic belt (eastern Cuba): Consequence of interaction between volatile-rich melts and peridotites in suprasubduction mantle. Econ. Geol. 94, 547–566.
Rassios, A., 1981. Geology and evolution of the magmatic rocks of the Vourinos ophiolite, northern Greece (Unpublished Ph.D. thesis). University of California, Davis, USA, pp. 1–594.
Rassios, A., Dilek, Y., 2009. Rotational deformation in the Jurassic Mesohellenic ophiolites, Greece, and its tectonic significance. Lithos 108, 207–223.
Rassios, A.E., Moores, E.M., 2006. Heterogeneous mantle complex, crustal processes, and obduction kinematics in a unified Pindos-Vourinos ophiolitic slab. In: Robertson, A.H.F., Mountrakis, D. (Eds.), Tectonic development of the eastern Mediterranean region. Geol. Soc. Am. Spec. Pap. 260, 237–266.
Rassios, A., Moores, E., Green, H., 1983. Magmatic structure and stratigraphy of the Vourinos ophiolite cumulate zone, northern Greece. Ofiol 8, 377–410.

Rollinson, P., 2008. The geochemistry of mantle chromitites from the northern part of the Oman ophiolite: inferred parental melt compositions. Contrib. Min. Petrol. 156, 273–288.
Saccani, E., Beccaluva, L., Coltorti, M., Siena, F., 2004. Petrogenesis and tectono-magmatic significance of the Albanide-Hellenide subpelagonian ophiolites. Ofiol 29 (1), 75–93.
Saccani, E., Beccaluva, L., Photiades, A., Zeda, O., 2011. Petrogenesis and tectono-magmatic significance of basalts and mantle peridotites from the Albanian-Greek ophiolites and sub-ophiolitic mélanges. New constraints for the Triassic-Jurassic evolution of the Neo-Tethys in the Dinaride sector. Lithos 124, 227–242.
Smith, A.G., Rassios, A., 2003. The evolution of ideas for the origin and emplacement of the western Hellenic ophiolites. Geol. Soc. Am. Spec. Pap. 373, 337–350.
Spray, J.G., Roddick, J.C., 1980. Petrology and 40Ar/39Ar geochronology of some Hellenic sub-ophiolitic metamorphic rocks. Contrib. Miner. Petrol. 72, 43–55.
Tzamos, E., Filippidis, A., Rassios, A., Grieco, G., Michailidis, K., Koroneos, A., Stamoulis, K., Pedrotti, M., Gamaletsos, P.N., 2016. Major and minor element geochemistry of chromite from the Xerolivado-Skoumtsa mine, Southern Vourinos: implications for chrome ore exploration. J. Geochem. Expl. 165, 81–93.
Vergely, P., 1976. Origine «vardarienne», chevauchement vers l'Ouest et rétrocharriage vers l'Est des ophiolites de Macédoine (Grèce) au cours du Jurassique supérieur-Eocrétacé. Comptes Rendus de l'Académie des Sciences 280, 1063–1066.
Wilson, M., 1989. Igneous Petrogenesis. Unwin Hyman, London, U.K., p. 466.
Zaccarini, F., Garuti, G., Proenza, J.A., Campos, L., Thalhammer, O.A.R., Aiglsperger, T., Lewis, J., 2011. Chromite and platinum-group-elements mineralization in the Santa Elena ophiolitic ultramafic nappe (Costa Rica): geodynamic implications. Geol. Acta 9, 407–423.
Zhou, M.F., Robinson, P.T., Malpas, J., Li, Z., 1996. Podiform chromitites from the Luobusa ophiolite (southern Tibet): implications for melt/rock interaction and chromite segregation in the upper mantle. J. Petrol. 37, 3–21.